Review article

Gas phase chemistry of neutral metal clusters: Distribution, reactivity and catalysis

Shi Yin, Elliot R. Bernstein*

Department of Chemistry, Colorado State University, Fort Collins, CO 80523, USA

ARTICLE INFO

ABSTRACT

Recent work on gas phase distribution, reactivity, and catalysis of neutral metal, metal oxide/carbide/sulfide clusters, investigated by single photon ionization coupled with time-of-flight mass spectrometry, is reviewed. Oxidation–reduction and bond activation reactions catalyzed by neutral metal and metal compound clusters are investigated, in order to understand the catalytic process at a molecular level, and reveal possible full catalytic cycles for related condensed phase reactivity and processes. Density functional theory calculations for these systems enable exploration of the geometric and electronic structures of clusters and determination of reaction intermediates and transition states, as well as reaction mechanisms, by comparing the results of theoretical calculations and experimental observations. Reactivity of metal oxide clusters with small gas phase molecules (CO, SO_2, and hydrocarbons), which is associated with the oxygen-rich or -deficient nature of the cluster, is discussed in terms of bond enthalpy, cluster spin state, and unpaired spin density of the clusters. For bond activation catalytic reactions on metal and metal compound clusters, we describe how adsorption of reactant molecules on active metal sites of clusters, association energy between reactant molecules and clusters, and activation energy (barriers) on the reaction potential energy surface can be constructed and compared to generate a reaction mechanism. Experimental and theoretical studies shown in this review also provide unique insights into how the application of gas phase neutral metal cluster chemistry is instructive in the understanding of important fundamental aspects of practical catalysis in the condensed phase.

© 2012 Elsevier B.V. All rights reserved.

Contents

---

* Corresponding author. Tel.: +1 970 491 6347.
  E-mail addresses: erb@lamar.colostate.edu, elliotbernst@gmail.com (E.R. Bernstein).

1. Introduction

Synthetic catalysts make a significant contribution to the production of all manufactured goods in all industrialized countries [1]; consequently, great efforts are undertaken to understand and improve the performance of catalysts by uncovering the detailed, microscopic geometrical and electronic structure of an active catalytic site, and the elementary steps comprising a catalytic reaction mechanism.

Transition metals, as well as their oxides, sulfides, and carbides, are unique in their abilities to catalyze chemical reactions, primarily due to their multiplicity of low energy surface electronic states, which can readily donate and/or accept electrons in the process of making and breaking bonds [2]. Transition metal oxides (TMOs) are employed extensively as catalysts in the petroleum, chemical, and environmental industries as heterogeneous catalysts and catalytic supports [3–10]. Members of the catalysis community, especially those concerned with solid inorganic catalysts, spend a good deal of their time interpreting the behavior and mode of action of existing catalysts, devising new method of probing catalysts under operating conditions, or contemplating ways to design new, more efficient catalysts.

The term "active site" first entered the literature of heterogeneous catalysis in the 1920s when H.S. Taylor suggested that monatomic steps or other topographical features such as fissures or troughs were likely to be the locus of enhanced catalytic activity. Catalytic properties of a material (activity, selectivity, and stability) are, in general, determined by chemical (electronic) properties of surface atoms/molecules [11,12]. On the basis of the concept that a catalytic reaction occurs at specific locally active sites [6,13,14], gas phase metal, metal oxide/sulfide/carbide clusters, which are composed of limited numbers of atoms, and which are fully accessible by both experiment and theory, are good model systems for the investigation of intrinsic reaction mechanisms for condensed phase catalytic processes [15–20]. With the absence of counterions and solvation, these gas phase ion and neutral clusters will, in general, be much more reactive than their condensed phase analogues [21–24], but such gas phase experimental studies, complemented by computational investigations, can provide a conceptual framework and an efficient means by which to obtain direct insight into reactivity patterns, the role of differential ligation, the importance of aspects of electronic structure, and the nature of crucial intermediates. On the other hand, studies of gas phase clusters can enable the identification of specific sites of reactivity for bulk condensed phase and surface systems. Discovery and elucidation of such cluster chemistry may shed light on design, synthesis, and more effective use of the related condensed phase catalysts.

Cluster electronic and reactivity properties should depend sensitively on charge state, especially for small clusters. Neutral cluster properties are important to study in order to have a complete understanding of a cluster, and by implication, of condensed phase and surface chemistry. Reactivity of both neutral and charged nanometer sized transition metal clusters has been extensively studied [25,26] since the pioneering work of Smalley and coworkers [27–29]. Ionic clusters [26,30] are easier to study by mass spectrometry, because electric and magnetic forces can be used to control and manipulate charged species; in contrast, neutral clusters are difficult to control and usually must be ionized for detection. The ionization of a neutral cluster by typical methods such as electron impact or multiphoton ionization techniques almost always causes cluster fragmentation. Cluster fragmentation during ionization prevents parent molecule identification because the different neutral clusters created are usually mixed together and their fragmentation patterns interfere with reactivity studies [31–33]. Single photon ionization (SPI) with vacuum ultraviolet (VUV) and soft X-ray or extreme UV (EUV) lasers has been recently demonstrated to be a successful technique for detecting neutral transition metals, as well as their oxides, sulfides, and carbides clusters without fragmentation [34–40].

Kappes and Staley's experimental investigation of CO oxidation by N_2O catalyzed by isolated FeO^+ (or Fe^+) in 1981 started the study of gas phase molecular heterogeneous catalysis [41]. After more than two decades, many examples of catalytic cycles facilitated by metal atoms [42–45], metal clusters [17,46,47], and metal oxide clusters [5,48–51] have been demonstrated. Several excellent reviews are available in the literature [30,52–55]. Meanwhile, reactivity of TMOs cluster ions toward various gas phase molecules has been extensively investigated with emphasis on understanding the important step(s), such as bond activation, in practical catalytic cycles [26,56–63]. Since mass spectrometric techniques are widely used for this research, most studies of TMOs cluster reactivity are for ionic TMOs clusters. Considerable experimental effort, however, has been expended to study the reactivity of neutral diatomic and polyatomic species by spectroscopic methods; for example, laser induced fluorescence (LIF) or infrared (IR) absorption studies have been reported for neutral species [64–67].

Neutral metal oxide/sulfide/carbide cluster distributions and reactivity were reported by our group, employing SPI with VUV and EUV lasers [36,40,68–75]. SPI is essential for detecting neutral oxide cluster distributions through time of flight mass spectrometry (TOFMS), while multiphoton ionization (MPI) through 193 and/or 355 nm laser radiation can never detect a complete metal oxide cluster distribution due to (sometimes severe) photo dissociation during or after ionization. As these gas phase studies can be performed under well-defined conditions, they play a key role in the evolution of approaches aimed at a more comprehensive understanding of the elementary reaction steps for catalytic mechanisms, knowledge of which is mandatory for the design of tailor made and improved catalysts.

In this review we focus on neutral metal and metal oxide/sulfide/carbide cluster gas phase distributions, reactivity, catalytic mechanisms, and provide unique insights into important fundamental aspects of practical catalysis in the condensed phase. We will discuss the chemistry of the following topics: (1) identification of neutral metal and metal oxide/sulfide/carbide clusters, (2) oxidation–reduction reactions catalyzed by metal oxide clusters, (3) chemisorption and bond activation catalysis with an emphasis on bond forming reactions, and (4) gas phase processes that enable understanding of the condensed phase catalytic process at a molecular level.

2. Experimental identification and spectroscopy of neutral metal clusters

Knowledge of the distribution of neutral metal clusters is an essential component for the elucidation of reactivity and catalytic behavior of such systems: the problem of cluster fragmentation in the process of their detection must therefore be addressed [10,22,76,77]. Since small metal oxide/sulfide/carbide clusters typically have an enormous density of vibronic states and very rapid relaxation processes, their spectra are often poorly resolved: their study and characterization are typically accomplished through mass spectrometry. Ionization of such neutral clusters is most gently done by photons, but multiphoton ionization can cause neutral cluster fragmentation and thus, loss of original cluster mass identity. The problem of cluster detection without interference from, or confusion generated by, parent neutral cluster fragmentation can be addressed in two ways: covariance mapping of the mass spectral data [32,33], and single photon ionization near threshold. In this review we focus on the latter approach, employing VUV lasers [78–85] (118 nm, 10.5 eV) and an EUV laser [35,86]

(46.9 nm, 26.5 eV). Some studies of emission [67,87–90], photo-electron [91–95], and vibrational [96,97] spectroscopies have been employed for the detailed characterization of small cluster structure and electronic states.

118 nm (10.5 eV) photons have two distinct advantages over other laser wavelengths that can be employed for cluster ionization: (1) a single 10.5 eV photon is energetic enough to ionize most metal oxide/sulfide neutral cluster and (2) at 10^{11}–10^{12} photons/pulse at 118 nm, the probability that any cluster will absorb more than one photon is vanishingly small. The distributions of neutral metal oxide, sulfide, or carbide clusters determined through photoionization time-of-flight (TOF) mass spectrometry, electronic spectroscopy, and density functional theory (DFT) calculations have been reported by Bernstein's group over the past decade [33–38,40,67,74,75,98–101].

The 532 nm laser ablation of metal foil in the presence of O_2, H_2S, or small hydrocarbon compounds in He is the widely employed method to generate metal oxide, sulfide, or carbide clusters [34,37,38,40,73,74]. Four different ionization laser wavelengths (355 nm, 193 nm, 118 nm and 46.9 nm) are usually employed for multiphoton and single photon ionization processes. Through these different ionization methods, the true neutral clusters distribution can be determined. The most intense features of the mass spectra of various metal oxide/sulfide neutral clusters obtained at different ionization laser wavelengths are summarized in Table 1. Comparison of the results obtained at 118 nm ionization (single photon) with those obtained at 193 nm and 355 nm ionization (through multiphoton processes) (in Table 1), leads to an understanding of the multiphoton neutral cluster fragmentation pathways. Fragment ion features are observed in the mass spectra of metal oxide/sulfide neutral clusters for only the 193 nm and 355 nm ionization schemes. The multiphoton fragmentation mechanism for these neutral metal oxide/sulfide clusters during the ionization process that seems most consistent with all the data is the loss of one or several oxygen or sulfur atoms. Using 10.5 eV, SPI for neutral clusters, with the possible relatively rare exception for clusters whose calculated ionization energy > 10.5 eV, almost all of these metal and metal compound clusters will be ionized. Most metal oxide/sulfide neutral clusters have ionization energies in the range 7–10.5 eV [37,38,67,75,100,102–105]. Thus, the cluster excess energy following ionization is ∼0–4 eV. This is not enough energy to break an M—O bond in the metal oxide cluster. Even 5–6 eV of excess energy in clusters would not yield fragmentation times (RRKM estimates) within the appropriate time range (∼<1 μs) for observable line width effects in large clusters. Multiphoton 355 and 193 nm ionization can of course cause fragmentation within this time range because many photons can be absorbed in the ionization process [32,33]. Two photon ionization, through a 355 nm (3.5 eV) plus 118 nm, (1 + 1) two photon process, for clusters with ionization energies larger than 10.5 eV is additionally possible, but should also not cause fragmentation of high ionization energy clusters. In general, for the majority of systems, the true neutral cluster distribution is obtained through 118 nm (or similar) single photon ionization, as verified by mass spectral peak line widths and calculations of the cluster binding energies, ionization energies, and fragmentation rates [35,37].

Employing TOFMS, single photon ionization at 193 nm can also be used to detect neutral metal carbon hydride ($Al_mC_nH_x$, $Mg_mC_nH_x$, $Be_mC_nH_x$, $Ca_mC_nH_x$) cluster distributions due to their low vertical ionization energies (VIEs) [40,74]. The metal carbon hydride clusters are generated through a metal ablation plasma–hydrocarbon reaction or an M–C ablation plasma reacting with H_2 gas. Only some of the neutral $M_mC_nH_x$ (M = Al, Mg, Be, Ca) clusters with odd mass numbers (i.e., an odd number of electrons), which have low VIEs, can be detected by SPI at 193 nm. Systematic variation of the VIEs of $M_mC_nH_x$ clusters with the numbers of M, C and H atoms is observed. VIEs of neutral $Al_2C_2H_x$ ($x = 0$–4), $Mg_2C_4H_x$ ($x = 0$–3), and $Be_2C_5H_x$ ($x = 0$–5) clusters systematically change with the number of H atoms (Fig. 1), because adding H atoms to the clusters changes the electronic configuration of the clusters from open shell to closed shell and vice versa. This study suggests that $M_mC_nH_x$ clusters have unique properties that make them a potential hydrogen storage material; for example, up to 13 wt% hydrogen storage by weight can be achieved for $Al_2C_2H_{12}$, and for a comparable Be molecule, the wt% H becomes close to 20%.

3. Catalytic reactions of neutral metal and metal compound clusters

3.1. Catalysis by metal oxide clusters: oxidation–reduction reactions

TMOs are widely used as heterogeneous catalysts or catalyst supports in the chemical industry [106,107]. Oxidation–reduction reactions over supported metal oxide catalysts represent a very important catalytic process in the chemical industry. Since processes on metal oxide catalytic surfaces are so complex, a fundamental understanding of these catalytic mechanisms is still not available, and thus a rational approach to effective catalyst synthesis and application is difficult. Gas phase studies of metal oxide clusters and their reaction behavior can help to understand the mechanism of elementary reactions in oxidation–reduction catalytic processes under isolated, controlled, reproducible, and theoretically predicated conditions [52,108–113].

Table 1
The most intense features of mass spectra of various metal oxide/sulfide/carbide neutral clusters obtained at different wavelength laser ionization.

Cluster	Most intense features obtained at different laser wavelength ionizations		
	355 nm	193 nm	118 nm
Cu_mO_n	$Cu_mO_{1,2}$	$Cu_{2m}O_m$ for $4 \leq m \leq 10$	Cu_mO_m ($m \leq 4$) and Cu_mO_{m-1} ($m > 4$)
Fe_mO_n	Fe_mO_m	Fe_mO_m, Fe_mO_{m+1}	Fe_mO_m, Fe_mO_{m+1}, and Fe_mO_{m+2}
Zr_mO_n	Zr_mO_{2m-1}	Zr_mO_{2m-1}	Zr_mO_{2m} and Zr_mO_{2m+1} for $m = 1$–30
M_mO_n (M = V, Nb, Ta)	M_mO_{2m} ($m = 2, 3$)	$M_mO_{m,m+1,2}$	$(MO_2)_x(M_2O_5)_y$ (x, $y = 0, 1, 2,...$)
Ti_mO_n	$Ti_mO_{2m-1,-2}$	$Ti_mO_{2m-1,-2}$	$Ti_mO_{2m,2m+1}$
Co_mO_n	–	–	$Co_mO_{m,m+1}$ ($m = 3$–5) $Co_mO_{m+2,m+3}$ ($m = 6$–9)
V_mS_n	–	V_mS_n, ($n \leq m + 1$)	V_mS_n ($n > m + 1$) $V_mS_nH_x$ ($x > 0$) are observed
Fe_mS_n	–	$Fe_mS_{m-1,m}$ ($m = 1$–6)	Fe_mS_m ($m = 2$–4) and $Fe_mS_nH_x$ ($n > m$, $x > 0$)
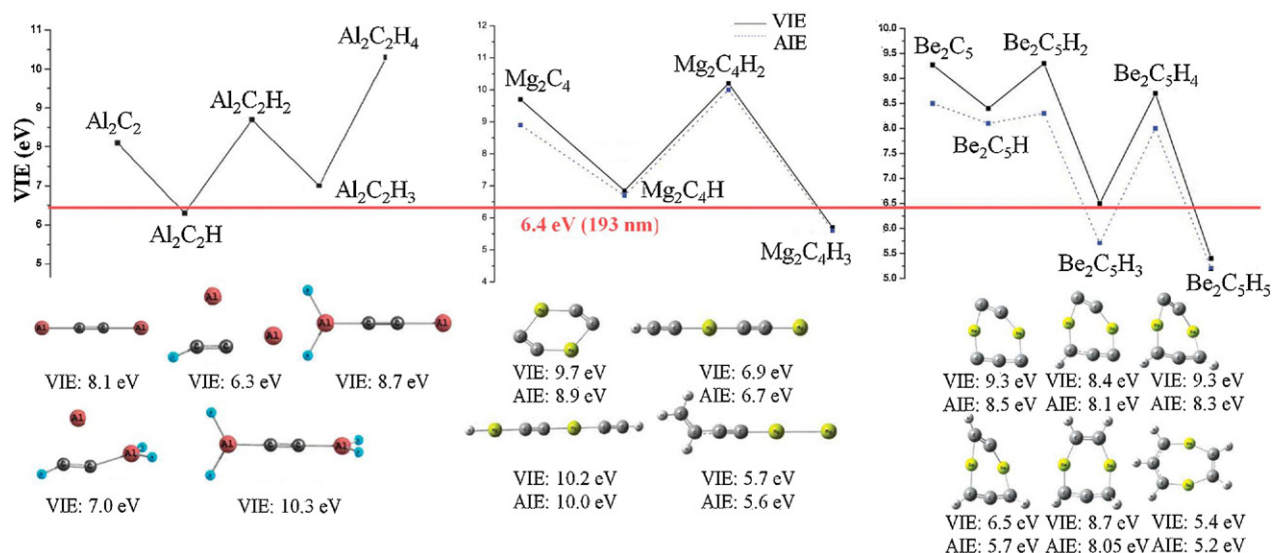
Fig. 1. The VIEs of $Al_2C_2H_{0-4}$ and the VIEs and AIEs of $Mg_2C_4H_{0-3}$, $Be_2C_5H_{0-5}$ clusters plotted against the number of H atoms x in the clusters. The structures under the plot are the lowest energy structures optimized at the MP2/6-311+G* theory level. Values (in eV) below each geometry are VIEs and AIEs for the clusters calculated at the same theory level.
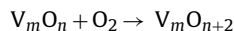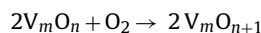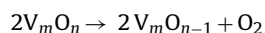Adapted from Refs. [40,74].

3.1.1. SO₂ oxidation

Vanadium oxide is a very important industrial heterogeneous catalyst [107,114–116]. V_2O_5 has been employed as a catalyst for oxidation of SO_2 to SO_3. Reactions of neutral vanadium oxide clusters with SO_2 were reported with the aim of elucidating a mechanism for the catalytic formation of SO_3 [72,117]. Many association reaction intermediates [$V_mO_nSO_2$ and $V_2O_4(SO_2)_2$] are observed. A weak feature at the SO_3 mass channel (80 amu) is suggested to be present in the product mass spectrum. Isolated SO is also observed as a product, as predicted by theoretical studies [117]. Both experiments and calculations suggest that SO_2 can be reduced and oxidized by oxygen-deficient and oxygen-rich clusters, respectively. The apparent activation energy for oxidation of SO_2 over a supported vanadium oxide catalyst is determined to be 21 ± 2 kcal/mol (=0.91 ± 0.09 eV) [118,119]. Considering the fact that VO_n represents an active site for a supported V_2O_5 catalyst [120], the model study shown in Fig. 2 reflects a possible mechanism for condensed phase catalysis; however, the activation energy (0.91 ± 0.09 eV) is interpreted as SO_3 desorption energy in the condensed phase studies. The calculated results (Fig. 2) indicate that this activation energy may mainly involve O—O bond cleavage for the VO_2O—OSO_2/VO_3SO_3 complex.
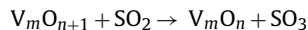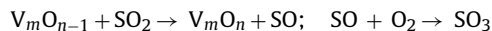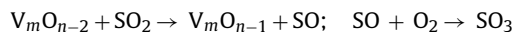
Three SO_3 formation mechanisms were also proposed based on experimental and calculational results [72].

Catalytic cycle I: SO and SO_3 formation occur on oxygen deficient and oxygen rich sites, respectively.

1. Formation of oxygen-deficient and oxygen-rich sites

$$2V_mO_n \rightarrow 2V_mO_{n-1} + O_2$$

$$2V_mO_n + O_2 \rightarrow 2V_mO_{n+1}$$

$$V_mO_n \rightarrow V_mO_{n-2} + O_2$$

$$V_mO_n + O_2 \rightarrow V_mO_{n+2}$$

2. Reactions of oxygen-deficient and oxygen-rich sites with SO_2 and regeneration:

$$V_mO_{n-2} + SO_2 \rightarrow V_mO_{n-1} + SO; \quad SO + O_2 \rightarrow SO_3$$

$$V_mO_{n-1} + SO_2 \rightarrow V_mO_n + SO; \quad SO + O_2 \rightarrow SO_3$$

$$V_mO_{n+1} + SO_2 \rightarrow V_mO_n + SO_3$$

Catalytic cycle II: SO and SO_3 formation occur on stable sites.

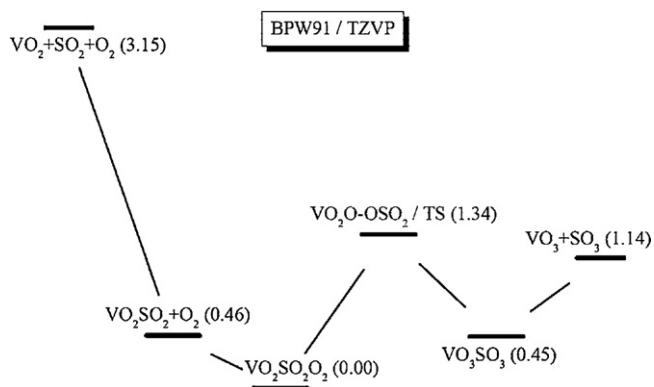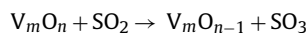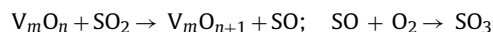1. Reactions of stable sites with SO_2, formation of oxygen-rich and oxygen-deficient sites:

$$V_mO_n + SO_2 \rightarrow V_mO_{n-1} + SO_3$$

Fig. 2. Schematic diagram showing SO_3 formation starting from three free gas molecules: VO_2, SO_2, and O_2. The values in parentheses are relative energies in eV. Note that these calculations are performed with the Gaussian 03 suite of programs and can be different from those of Gaussian 98 by as much as (0.05 eV).
From Ref. [72].

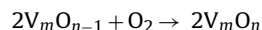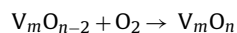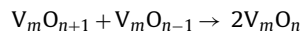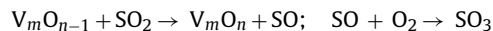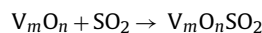$$V_mO_n + SO_2 \rightarrow V_mO_{n+1} + SO; \quad SO + O_2 \rightarrow SO_3$$

2. Regeneration of stable sites:

$$V_mO_{n-1} + SO_2 \rightarrow V_mO_n + SO; \quad SO + O_2 \rightarrow SO_3$$

$$V_mO_{n+1} + V_mO_{n-1} \rightarrow 2V_mO_n$$

$$V_mO_{n-2} + O_2 \rightarrow V_mO_n$$

$$2V_mO_{n-1} + O_2 \rightarrow 2V_mO_n$$
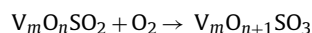
$$V_mO_{n+1} + SO_2 \rightarrow V_mO_n + SO$$
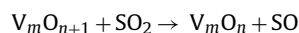
Catalytic cycle III: SO_3 formation occurs on stable sites through oxidation by both O_2 and catalyst.

1. Formation of reaction intermediate from a stable site:

$$V_mO_n + SO_2 \rightarrow V_mO_nSO_2$$

2. Oxidation of a reaction intermediate by O_2 and SO_3 formation:

$$V_mO_nSO_2 + O_2 \rightarrow V_mO_{n+1}SO_3$$

3. Regeneration of a stable site:

$$V_mO_{n+1} + SO_2 \rightarrow V_mO_n + SO_3$$

$$2V_mO_{n+1} \rightarrow 2V_mO_n + O_2$$
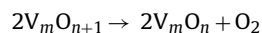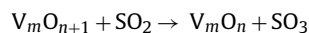
3.1.2. CO oxidation

Low-temperature, low-cost, and efficient CO oxidation (removal) can solve serious environmental problems that are caused by CO emission from automobiles, industrial processing, and even cigarette burning. CO oxidation is also important in other areas such as respiratory protection and fuel gas cleanup. Gold based catalysts are employed for low temperature CO oxidation [121], and have been studied extensively in the condensed phase [122–129] and in the gas phase [130–134], but a search for alternative, low-cost, and noble metal free materials has led to the study of transition metal and metal oxide catalysts [135–138] for such reactions. In the following we present three studies dealing with the oxidation reactions of CO catalyzed by neutral gold clusters, iron oxide, and cobalt oxide clusters.

Experimental and theoretical studies of the oxidation reaction of neutral $Au_m(CO)_n$ clusters in the gas phase are undertaken through single photon ionization TOFMS at 193 nm [139]. Neutral gold carbonyl clusters, $Au_m(CO)_n$ ($m = 3–9$, $n = 2–7$, $m \geq n$), are generated by laser ablation of Au into a mixture of CO/He, cooled by expansion and collision with He, and reacted, with both O_2 and N_2O in a fast flow reactor. $Au_3(CO)_2$, $Au_5(CO)_4$ and $Au_7(CO)_5$ neutral clusters are especially reactive with O_2, while neutral clusters $Au_3(CO)_3$ and $Au_7(CO)_4$ are only moderately reactive with O_2. With possible minor exceptions for $Au_3(CO)_2$ and $Au_3(CO)_3$, none of the $Au_m(CO)_n$ neutral clusters studied in the experiments prove to be reactive with N_2O. A complete mechanistic catalytic cycle was suggested
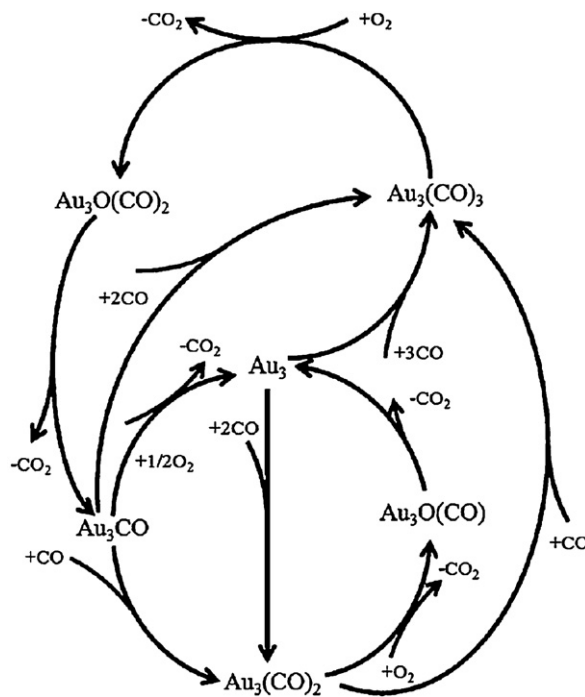

Fig. 3. Schematic representation of the catalytic cycle for CO oxidation to CO_2 by O_2 on the Au_3 cluster.
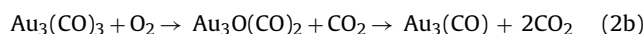From Ref. [139].

for the gold catalyzed, low temperature oxidation of CO to CO_2. The full cycle is composed of a number of possible elementary reactions as shown in Fig. 3. The catalytic cycle incorporates the following reactions:
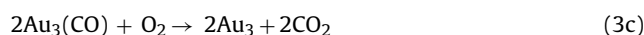
(1) Adsorption

$$Au_3 + 2CO \rightarrow Au_3(CO)_2 \tag{1a}$$

$$Au_3 + 3CO \rightarrow Au_3(CO)_3 \tag{1b}$$

(2) Reaction

$$Au_3(CO)_2 + O_2 \rightarrow Au_3O(CO) + CO_2 \rightarrow Au_3 + 2CO_2 \tag{2a}$$

$$Au_3(CO)_3 + O_2 \rightarrow Au_3O(CO)_2 + CO_2 \rightarrow Au_3(CO) + 2CO_2 \tag{2b}$$

(3) Regeneration

$$Au_3(CO) + CO \rightarrow Au_3(CO)_2 \tag{3a}$$

$$Au_3(CO) + 2CO \rightarrow Au_3(CO)_3 \tag{3b}$$

$$2Au_3(CO) + O_2 \rightarrow 2Au_3 + 2CO_2 \tag{3c}$$

Single photon ionization (118 nm) and DFT calculations are also successfully applied for the investigation of CO oxidation with small neutral iron oxide clusters ($FeO_{1–3}$ and $Fe_2O_{4,5}$) [140]. FeO_2 and FeO_3 neutral clusters are reactive toward CO, whereas Fe_2O_4, Fe_2O_5, and possibly FeO are not reactive. A higher reactivity for FeO_2 [$\sigma(FeO_2 + CO) > 3 \times 10^{-17}$ cm^2] than for FeO_3 [$\sigma(FeO_3 + CO) \sim 1 \times 10^{-17}$ cm^2] is observed. The reaction is driven by additional C═O bond formation which is facile due to favorable thermodynamics: CO_2 (O─CO) bond enthalpy (5.54 eV) is higher than those of $FeO_{1–3}$ and $Fe_2O_{4,5}$ (2.93–4.29 eV).

The three catalytic cycles (I–III) for CO oxidation by O_2 facilitated by $FeO_{1–3}$, $Fe_2O_{3–5}$, and $Fe_2O_{2–4}$ clusters are presented in Fig. 4: FeO_3 oxidizes CO to produce FeO_2 and CO_2, FeO_2 oxidizes CO to produce FeO and CO_2; the O–O bond of O_2 then breaks on FeO to regenerate FeO_3, with the addition of two Fe─O bonds. Each of
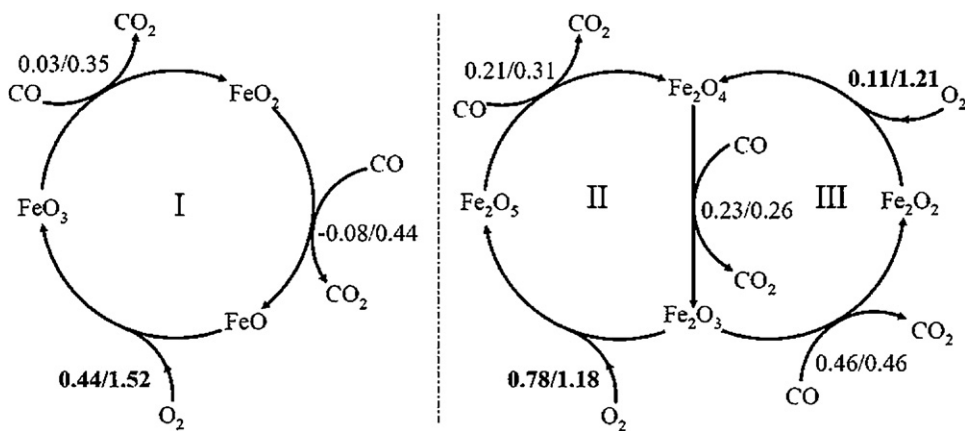
Fig. 4. Three model catalytic cycles for the CO oxidation by O_2 over FeO_{1-3} and Fe_2O_{2-5}. The overall reaction barrier (ΔG_{ORB}) and the corresponding absolute reaction barrier (ΔG_{ARB}) in eV for each elementary step are given as $\Delta G_{ORB}/\Delta G_{ARB}$.
From Ref. [140].

the O—O bond breaking process is subject to a high absolute reaction barrier (ARB), defined as the energy difference between the transition state (TS) and the intermediate through which the TS is generated. The rate limiting steps of cycles I and II are the O—O bond activation (or breaking) processes that are subject to both high overall reaction barriers (ORBs) and ARBs. The rate-limiting step of cycle III is not apparent because the O—O ($Fe_2O_2 + O_2 \rightarrow Fe_2O_4$) activation has a smaller ORB and a much higher ARB than the Fe—O activation (such as, $Fe_2O_3 + CO \rightarrow Fe_2O_2 + CO_2$) does.

The mechanism for the oxidation of CO to form CO_2 over an iron oxide catalyst involves interaction of a lone pair of electrons from carbon with an iron atom and subsequent activation of an Fe—O bond to initiate formation of another C=O bond. Two essential steps are present in the oxidation of CO by Fe_mO_n clusters: (1) initial intermediate formation that involves carbon–iron interaction and (2) Fe—O bond activation that determines the overall reaction barrier. The Fe—O bond activation energy at room temperature varies from -0.08 (FeO_2) to 0.46 eV (Fe_2O_3). The process of the O—O bond breaking on FeO is the rate-limiting step, which suggests that efficient O_2 activation should be considered in practical catalysis.

The study of CO oxidation by Co_mO_n clusters has shown that the Co_3O_4 cluster has the highest reactivity for reactions with CO [68]. Cluster reactivity is highly correlated with the following factors: cluster size, Co(III) concentration in the cluster, the number of the cobalt atoms with high oxidation states, and the presence of an oxygen molecular moiety (an O—O bond) in the Co_mO_n cluster.

The potential energy surface (PES) along the reaction coordinate for the reaction of Co_3O_4 with CO was calculated at the DFT BPW91/TZVP level of theory (Fig. 5). The Co_3O_4 cluster has C_{2v} symmetry with doublet and quartet spin multiplicities: the doublet conformer is higher in energy than the quartet conformer by 0.10 eV. DFT calculations predict bond lengths of 1.761 Å for Co(II)—O and 1.801 Å for Co(III)—O in $^2Co_3O_4$, with two parallel oxygen bridges between two Co(III) atoms (see Fig. 5). The product Co_3O_3 has a C_s symmetry, with the doublet conformer slightly higher in energy than the quartet conformer by 0.10 eV. CO_2 is formed linearly on the Co_3O_4 cluster through a transition state TS1 (-0.52 eV for the doublet and -0.45 eV for the quartet), indicating that the CO molecule attacks one of the parallel bridge oxygen atoms between the two Co(III) atoms. The transition state TS1 involves cleavage of two Co(III)—O bonds and elongation of the Co(II)—C bond. The overall reaction $Co_3O_4 + CO \rightarrow Co_3O_3 + CO_2$ is exothermic (-2.16 eV for the doublet and -2.27 eV for the quartet), and thermodynamically barrierless.

As seen in the Co_3O_4 cluster unpaired spin density profile in Fig. 6, unpaired electrons are mostly localized on the Co(II) site,

which is the most active site in the Co_3O_4 cluster. The lowest energy conformer structure for the association product Co_3O_4CO has CO bonded to the Co(II) site. Since Co(II) is a more unpaired electron rich site than Co(III), CO bonding to the cluster Co(II) site is reasonable according to well established metal carbonyl chemistry. For Co_3O_4CO, unpaired electrons are localized at the two Co(III) atoms and the two bridge oxygen atoms (see Fig. 6). Therefore the bridge oxygen atoms have major responsibility for the high reactivity of the Co_3O_4 cluster for CO oxidation. Generally, for CO oxidation, one oxygen atom in CO_2 is from a bridge oxygen connected to the two Co(III) atoms, and these two Co(III)s are thereby reduced to Co(II)s in the product Co_3O_3.

Overall, CO is predicted to be adsorbed on the Co(II) site, and react with one of the parallel bridge oxygen atoms between two Co(III) atoms in the Co_3O_4 cluster. The oxidation reactivity is indicated to be associated with appropriate Co(III) concentration, and the number of cobalt atoms with high oxidation states or O—O bonding moieties in the cobalt oxide clusters. The Co_3O_4 cluster has the highest overall rate constants for oxidation of CO (1.62×10^{-12} cm^3 s^{-1}).
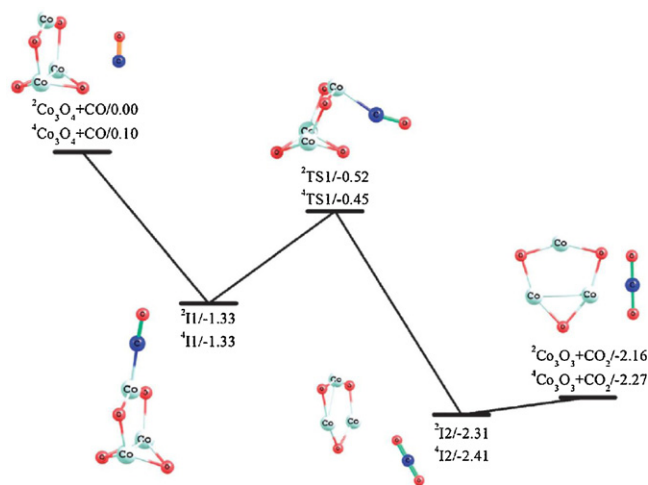
Fig. 5. Reaction pathway for $^{2/4}Co_3O_4 + CO \rightarrow {}^{2/4}Co_3O_3 + CO_2$ calculated at the BPW91/TZVP level. The reaction intermediates and transition states are denoted as ^MI_n and ^MTS_n, respectively, in which the superscript M indicates the spin multiplicity. Energies, including ZPE corrections, are given in eV and are relative to the initial energy of the $^2Co_3O_4 + CO$ reactants. Cobalt atoms are the lightest in color, followed by oxygen, and carbon as the darkest.
From Ref. [68].

Fig. 6. Unpaired spin density profiles for Co_3O_4 and Co_3O_4CO clusters. Adapted from Ref. [68].

3.1.3. Methanol oxidation to formaldehyde

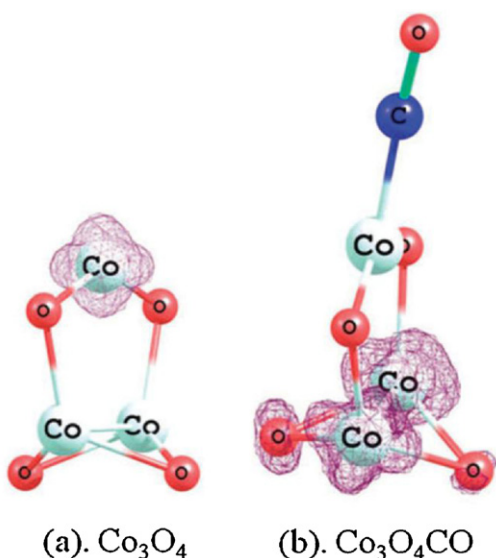Methanol as a clean energy resource can be used directly for transportation or can be added to the conventional fossil fuels [141,142]. Commercially, methanol is synthesized from carbon monoxide and hydrogen [143,144], and almost 40% of the produced methanol is converted to formaldehyde over iron molybdenum oxide catalysts [145,146]. The reaction enthalpy for methanol selective oxidation to formaldehyde is $CH_3OH + 1/2O_2 \rightarrow CH_2O + H_2O$ ($\Delta H = -153$ kJ/mol) (http://webbook.nist.gov/chemistry). Dehydrogenation of methanol over TMOs in the gas phase has been extensively investigated; most researchers focus on the reactions of cation or anion metal oxide clusters [59,147–154].

Reactions of neutral iron oxide clusters with methanol were studied by TOFMS employing 118 nm SPI and DFT calculations [69]. Methanol dehydrogenation reactions are observed for $FeO_{1,2}$ and Fe_2O_{2-5} clusters. DFT calculations are additionally performed and the following conclusions can be drawn from the theoretical studies: (1) the O—H bond of methanol is more readily activated by iron oxide than the C—H bond of the methyl group, and hydrogen transfer from the O—H group occurs prior to that from the C—H group; (2) neutral water elimination reactions are energetically more favorable than dehydrogenation reactions on iron oxide clusters; and (3) neutral formaldehyde CH_2O is suggested to be generated from the reactions of $FeO_{1,2}$ and Fe_2O_{2-5} with CH_3OH at room temperature based on experimental observations.

The catalytic cycles are suggested and presented in Fig. 7. FeO_3 and FeO_2 can be reduced to FeO_2 and FeO, respectively, by CH_3OH to form $CH_2O + H_2O$, and the generated FeO is subsequently reoxidized by O_2, and FeO_3 is regenerated (cycle a). In a reaction similar to the $FeO_3/FeO_2/FeO$ cycle, methanol can be oxidized by Fe_2O_5 and Fe_2O_4 clusters, and the generated Fe_2O_3 can be oxidized to Fe_2O_5 by O_2 (cycle b).

Reactions of charged Fe_mO_n clusters with methanol have also been investigated experimentally [152,153,155] and theoretically [151]. Four types of ion reactions are identified for the overall reaction of FeO^+ with methanol [155]. All four reactions are exothermic based on thermochemistry data [155] and DFT calculational results [151].
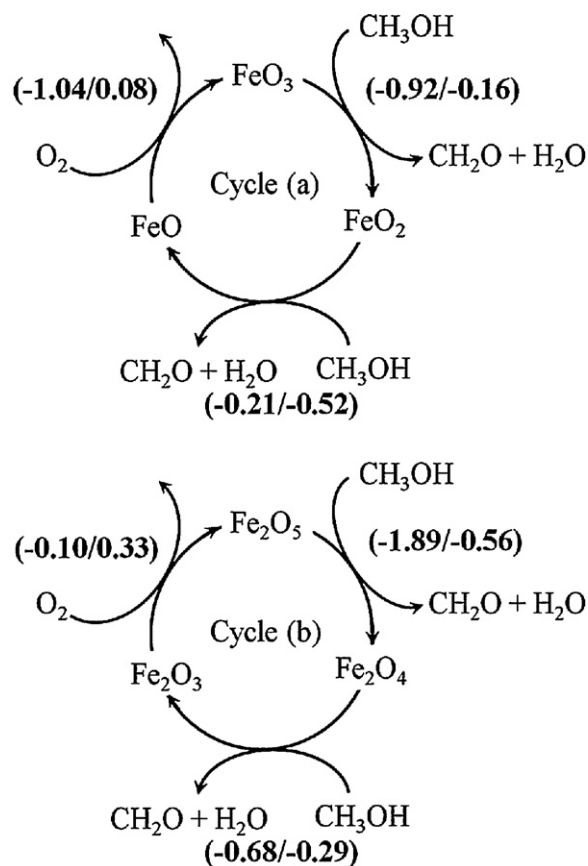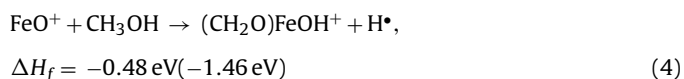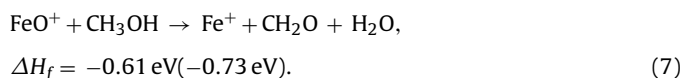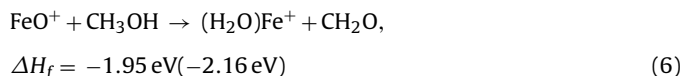
$$FeO^+ + CH_3OH \rightarrow (CH_2O)FeOH^+ + H^\bullet,$$
$$\Delta H_f = -0.48\,eV(-1.46\,eV) \tag{4}$$

Fig. 7. Proposed catalysis cycles for the reaction $CH_3OH + 1/2O_2 \rightarrow CH_2O + H_2O$ over (a) $FeO_3/FeO_2/FeO$ and (b) $Fe_2O_5/Fe_2O_4/Fe_2O_3$ clusters. Reaction energies (a) and overall barriers (b) are listed for each reaction as (A/B) in eV. From Ref. [69].

$$FeO^+ + CH_3OH \rightarrow (CH_2O)Fe^+ + H_2O,$$
$$\Delta H_f = -2.04\,eV(-1.93\,eV) \tag{5}$$

$$FeO^+ + CH_3OH \rightarrow (H_2O)Fe^+ + CH_2O,$$
$$\Delta H_f = -1.95\,eV(-2.16\,eV) \tag{6}$$

$$FeO^+ + CH_3OH \rightarrow Fe^+ + CH_2O + H_2O,$$
$$\Delta H_f = -0.61\,eV(-0.73\,eV). \tag{7}$$
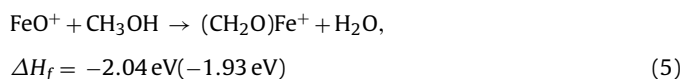
The related neutral cluster reaction energies are calculated by DFT as [69]

$$^5FeO + CH_3OH \rightarrow {}^4(CH_2O)FeOH + H\cdot, \quad \Delta E = 0.37\,eV \tag{8}$$

$$^5FeO + CH_3OH \rightarrow (CH_2O)^5Fe + H_2O, \quad \Delta E = -0.18\,eV \tag{9}$$

$$^5FeO + CH_3OH \rightarrow H^5FeOH + CH_2O, \quad \Delta E = -0.86\,eV \tag{10}$$

$$^5FeO + CH_3OH \rightarrow {}^5Fe + CH_2O + H_2O, \quad \Delta E = 0.38\,eV \tag{11}$$
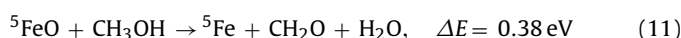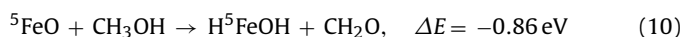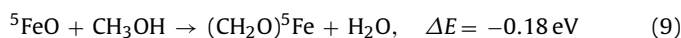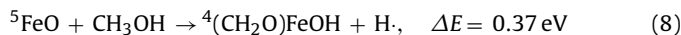
The product distribution for cationic (Reactions (4)–(7)) FeO^+ and neutral FeO cluster reactions (Table 2) with methanol are different: $FeOH$, $(CH_2O)FeOH$, and association product $Fe_mO_nCH_3OH$, are observed only for the neutral cluster reactions, and are not present for cationic reactions. Hydrogen radical generation is favorable for cationic cluster reaction (4), but unfavorable for the neutral cluster reaction (8). For Reaction (10), the neutral intermediate

Table 2
Observed product for the reactions of neutral iron oxide clusters with CH_3OH and CD_3OH.

Mass	CH_3OH	Mass	CD_3OH
73	FeOH	...[a]	...
74	HFeOH	75	FeOHD
86	$(CH_2O)Fe$	88	$(CD_2O)Fe$[b]
90	$(H_2O)FeO$	91	$(HDO)FeO$
103	$(CH_2O)FeOH$[a]	...[a]	...
104	$FeOCH_3OH$[c]	107	$FeOCD_3OH$
118	$FeOC_2H_6O$[d]	124	$FeOC_2D_6O$
145	Fe_2O_2H	...[a]	...
146	$Fe_2O_2H_2$	147	Fe_2O_2HD
162	$Fe_2O_3H_2$	163	Fe_2O_3HD
178	$Fe_2O_4H_2$	179	Fe_2O_4HD
194	$Fe_2O_5H_2$	195	Fe_2O_5HD

Ref. [69].
[a] The related deutrated species signals are too weak to be positively identified.
[b] Overlapped with FeO_2 in mass number.
[c] Overlapped with FeO_3 in mass number.
[d] Overlapped with FeO_2CH_2O in mass number.

structure (HO)—(H)Fe(OCH$_2$) (Fig. 8, structure 8) is more stable than its conformer structure $(H_2O)Fe(OCH_2)$ by 0.90 eV, and the following dissociation product, (H)Fe(OH), for which both hydrogen and the hydroxyl group are bonded to the Fe atom, is also more stable than $(H_2O)Fe$ (by 0.81 eV). As a comparison, $(H_2O)Fe^+(OCH_2)$ is the most stable structure and $(H_2O)Fe^+$ is the most stable dissociation product for the related cationic reaction (5) [151]. Thus, even though the product mass numbers are the same for the reactions of FeO or FeO$^+$ with methanol, the product structures and reaction pathways are significantly different based on DFT calculations.

Reactions of anionic FeO$_2^-$, Fe$_2$O$_3^-$, and Fe$_2$O$_4^-$ with methanol and deutrated methanol have also been investigated [153]. Observations of FeO$_2$HD$^-$ by employing deutrated methanols, CH$_3$OD, and CD$_3$OH, indicate that the hydrogens of FeO$_2$H$_2^-$ are from both O—H and C—H groups; this is consistent with the neutral cluster studies [69]. The structure of FeO$_2$H$_2^-$ is suggested as Fe(OH)$_2^-$, however, with two hydroxyl groups bonded to the Fe atom, whereas the most stable structure for neutral species is calculated as $(H_2O)FeO$, suggesting a different reaction mechanism for

Fig. 8. Reaction pathways for $^5FeO + CH_3OH \rightarrow H^5FeOH + CH_2O$ calculated at the B3LYP/6-311+G(d) level. Energies are relative to the energy of the $^5FeO + CH_3OH$ reactants. The solid line indicates hydrogen transfer to the oxygen atom of FeO from the O—H group, and the dashed dot line indicates hydrogen transfer to the iron atom of FeO from the O—H group. R3: $^5FeO + CH_3OH$; P3: $H^5FeOH + CH_2O$. Iron, oxygen, carbon, and hydrogen are in pink, red, dark blue, and light blue, respectively. From Ref. [69]. (For interpretation of the references to color in this figure legend, the reader is referred to the web version of the article.)

anionic and neutral cluster reactions. Secondary reaction products for Fe(OH)$_2^-$ have also been obtained, which imply the reaction $FeO_2H_2^- + CH_3OH \rightarrow FeO_3^- + H_2 + CH_4$ occurs; however, the reaction energy for related neutral $(H_2O)FeO$ cluster reaction is calculated as 2.47 eV. This high reaction energy clearly indicates that the secondary reaction does not occur.

Oxidation of methanol to formaldehyde by FeO^{2+} in the gas phase and in the solution has also been calculated by DFT [152]. Interestingly, hydrogen transfer from the C—H group of methanol followed by that from the O—H group, is given as the most likely mechanism. In addition, the product structure, $(H_2O)Fe^{2+}$, which is similar to $(H_2O)Fe^+$ with a water molecule bonded to the Fe atom through the O atom, is different from the related neutral species HFeOH.

3.1.4. Hydrocarbon oxidation

The oxidation of hydrocarbons over supported metal oxide catalysts is a very important catalytic process in the chemical industry. For example, catalytic partial oxidation of propylene (CH$_2$=CHCH$_3$) produces acrolein (CH$_2$CHCHO), one of the more employed industrial chemical intermediates [156–158]. The reaction mechanism of neutral vanadium oxide clusters with hydrocarbons (e.g., ethane, ethylene, and acetylene) are investigated employing 26.5 eV soft X-ray laser and 10.5 eV nm laser ionization TOFMS [70,159], in combination with DFT calculations [160]. The reactivity for neutral vanadium oxide clusters (V$_m$O$_n$) toward C$_2$H$_6$, C$_2$H$_4$, and C$_2$H$_2$ is found to increase with degree of unsaturation of the hydrocarbon. This reactivity trend is well associated with the behavior of binding energies between these hydrocarbons and V$_m$O$_n$ clusters. For example, the saturated hydrocarbon C$_2$H$_6$ bonds weakly (0.65 eV) with V$_2$O$_5$, whereas C$_2$H$_4$ and C$_2$H$_2$ bond more strongly with V$_2$O$_5$ by CO and VC chemical bonds at 1.33 and 2.5 eV (Fig. 9).

C$_2$H$_6$ (C$_n$H$_{2n+2}$, saturated) molecules are not reactive with neutral vanadium oxide clusters at low temperatures (reactants and products are thermalized to 300–400 K by collision after the reaction [28]). Since the reactions $C_nH_{2n+2} \rightarrow C_{n-1}H_{2n-2} + CH_4$ are endothermic ($\Delta H > 0$), saturated hydrocarbon molecules may be reactive at high temperature, when $\Delta G_{react} < 0$. For the reaction of V$_m$O$_n$ + C$_2$H$_4$, products VO$_2$CH$_2$, V$_3$O$_7$CH$_2$, and V$_5$O$_{12}$CH$_2$, in additional to association products are observed. C=C bond cleavage occurs for C$_2$H$_4$ reacting with the oxygen rich neutral clusters VO$_3$, V$_3$O$_8$, and V$_5$O$_{13}$. For the V$_m$O$_n$ + C$_2$H$_2$ reactions, association reactions are identified as the major products. Two dehydration products VO$_2$C$_2$ and VOC$_4$H$_2$ are also identified. DFT calculated results suggest that both reaction channels, dehydration (water formation) and partial oxidation (ketene formation), can occur without an overall reaction barrier for the VO$_3$ + C$_2$H$_2$ reaction.

The cleavage of C=C bonds of alkenes on oxygen rich neutral V$_m$O$_n$ clusters is a unique reaction. C=C bond breaking only happens on oxygen rich vanadium oxide clusters with an odd number of vanadium atoms, and the overall stoichiometry VO$_3$(V$_2$O$_5$)$_n$, $n = 0$, 1, 2,.... By DFT calculation, VO$_3$ and V$_3$O$_8$ are demonstrated to be less stable clusters than VO$_2$ and V$_3$O$_7$, respectively [98]. The excess oxygen in oxygen rich metal oxide clusters can be considered an oxygen centered radical site in the cluster. DFT calculations show that VO$_3$ associates with C$_2$H$_4$ to form a stable five membered ring intermediate. A large amount of energy (2.12 eV) is then released, leading to C=C bond breaking. A V$_3$O$_8$ structure (shown in Fig. 10) can be generated from V$_2$O$_5$ bonded to VO$_3$ for a model structure of (V$_2$O$_5$)(VO$_3$), in which V and O atoms of the V$_2$O$_5$ moiety are in oxidation states +5 and −2, respectively. Density functional theory calculations of the reaction mechanisms for V$_3$O$_8$ + C$_2$H$_4$ [161] also suggest that the (O$_b$)$_2$V(O$_t$O$_t$)$^\bullet$ moiety contains the radical oxygen center in V$_3$O$_8^\bullet$. O$^\bullet$ is the active site for reaction toward C$_2$H$_4$ oxidation. Similar reactivity has been identified for the (O$_b$)$_2$V(O$_t$O$_t$)$^\bullet$ sites in V$_3$O$_8$ and the VO$_3^\bullet$ cluster [(O$_t$)$_2$VO$_t^\bullet$]: in this instance
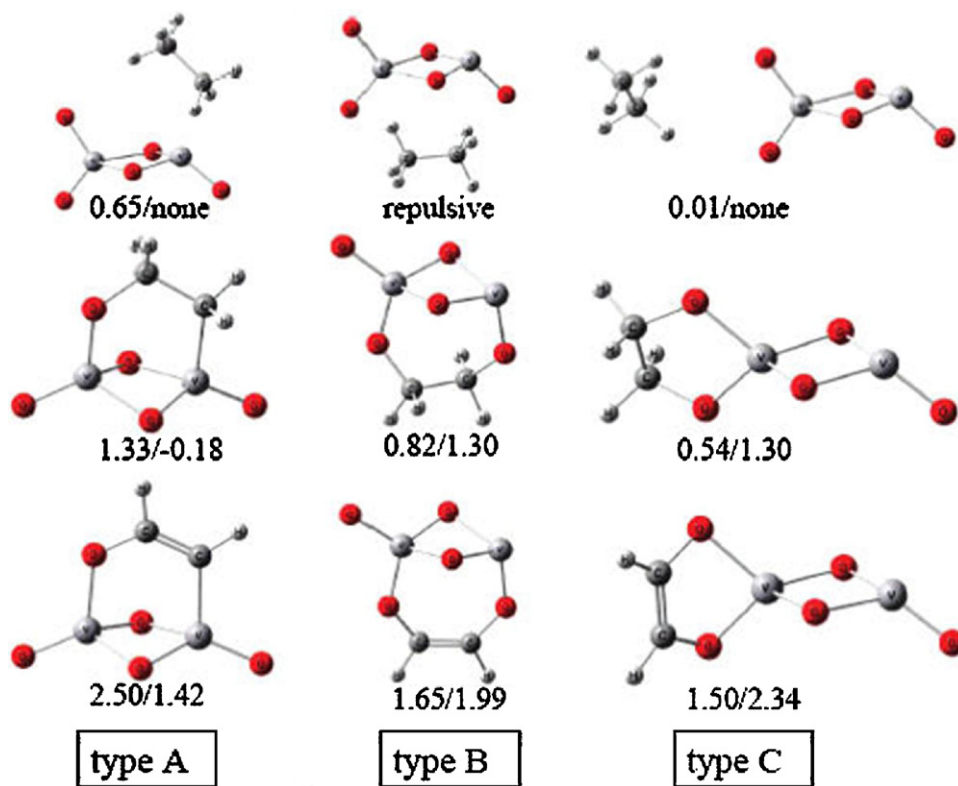
Fig. 9. DFT optimized geometries of association products $V_2O_5C_2H_x$ ($x = 6$ (top), 4 (middle), and 2 (bottom)). Three types of geometry configurations (A, B, C) are presented. The values $x1/x2$ below each geometry are the zero-point vibrational energy corrected binding energies, in which $x1$ and $x2$ are the values for the association species in singlet and triplet spin states, respectively.
From Ref. [159].

to enable C=C bond cleavage of C_2H_4. Thus, oxygen rich vanadium oxide clusters VO_3, V_3O_8, V_5O_{13}, etc. can be expressed as $VO_3(V_2O_5)_n$, $n = 0, 1, 2, \ldots$. These clusters have an oxygen centered radical (VO_3), which can surmount the barrier associated with formal [3 + 2] cycloaddition.

Note that C=C bond breaking for C_2H_4 does not occur for (1) the most stable V_mO_n (e.g., VO_2, $V_2O_{4,5}$, $V_3O_{5,6,7}$) clusters [98], (2) oxygen rich V_mO_n clusters with an even number of V atoms, (3) other metal oxide clusters, such as Nb_mO_n, Ta_mO_n, Ti_mO_n, Co_mO_n, Si_mO_n, Fe_mO_n, Hf_mO_n, Zr_mO_n, and (4) vanadium oxide cluster ions ($V_mO_n^\pm$). These results indicate that the activities of metal oxide clusters are dependent on many issues: bond energies, reaction barriers, reaction rates, etc., not only on the oxygen-rich or -poor nature of M_mO_n clusters.

On the basis of experimental data and DFT calculations, a catalytic cycle for oxidation of alkenes to produce formaldehyde and other aldehydes on vanadium oxide clusters is suggested (Scheme 1). Since VO_3 can thereby be employed in a catalytic cycle for C_2H_4 oxidation to H_2CO, other larger clusters of this general type ($VO_3(V_2O_5)_n$, $n = 0, 1, 2, \ldots$) can be active in a similar fashion.

3.2. Chemisorption and bond activation catalysis

The concept of catalysis through bond activation by neutral metal clusters in gas phase processes refers to situations for which the catalytic neutral metal cluster simply activates a relevant part
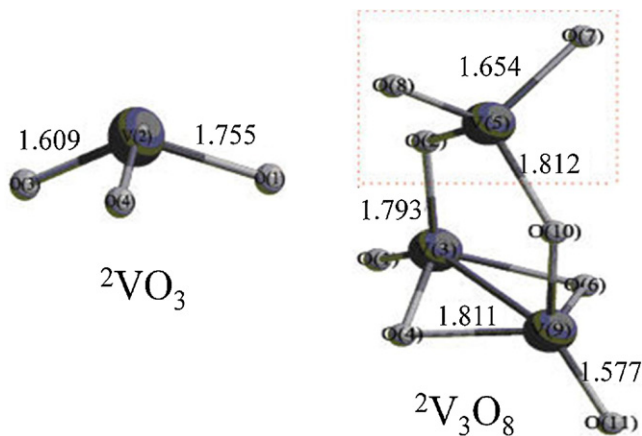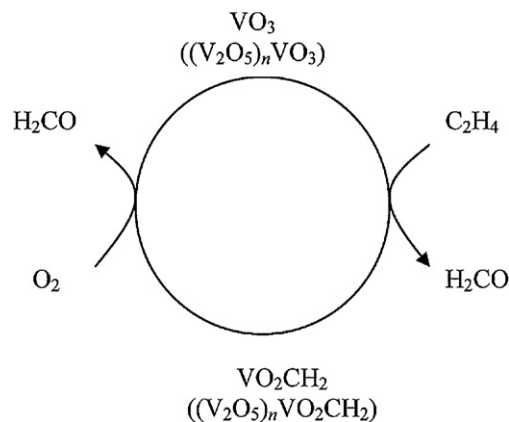

Fig. 10. DTF calculated the lowest energy structures of VO_3 and V_3O_8 at B3LYP/TZVP level.
From Ref. [159].

Scheme 1. Ref. [159].

of the reagent sufficiently and transfers the activated fragment to a second chemisorbed (activated) molecule on the catalytic metal cluster. Three examples from different areas will be included in this section.

3.2.1. $Nb_8 + CO + 2H_2$

The first such catalysis was demonstrated for methanol synthesis from carbon monoxide and hydrogen. This reaction, $CO + 2H_2 \rightarrow CH_3OH$ ($\Delta H_{298} = -91$ kJ/mol), is an important industrial process, and it offers a clear economic and political advantage compared with oil refining [144]. Reaction of CO with H_2 on neutral V_n, Nb_n, and Ta_n clusters in the gas phase is explored by employing TOFMS with 193 nm single photon ionization [71]. A strong size dependent reactivity of Nb_n toward CO, H_2, and CH_3OH is characterized. A stable product Nb_8COH_4 is identified for reactions of both $Nb_n + CO + H_2$ and $Nb_n + CH_3OH$, which suggests that CH_3OH is formed on the Nb_8 cluster through reaction of $Nb_8 + CO + 2H_2$. For all other V_n, Nb_n ($n \neq 8$), and Ta_n clusters, either the hydrogen transfer barrier is high so that CH_3OH formation does not occur or the hydrogen transfer barrier is low enough so that CH_3OH is formed, but it is not preserved on the clusters due to a low dehydrogenation barrier.

CH_3OH can be generated on Nb_8 by the reaction $Nb_8 + CO + 2H_2 \rightarrow Nb_8COH_4 \rightarrow Nb_8 + CH_3OH$ ($\Delta H = -1.05$ eV) based on DFT calculations as presented in Fig. 11. The first step, molecular adsorption of CO on the Nb_8 cluster to form Nb_8CO, is an exothermic reaction. Via transition state TS0, the molecular adsorption product Nb_8CO can transform to a dissociative adsorption product CNb_8O, thereby inhibiting the desired Nb_8 supported reaction, $CO + 2H_2 \rightarrow CH_3OH$. Thus, dissociative or molecular adsorption strongly depends on the details of the metals and adsorbed molecules [131,162]. An H_2 adsorption channel for dissociation of one hydrogen molecule on Nb_8 and formation of Nb_8HHCO is available, and it is a more favorable pathway with H_2 molecules present in the reaction.

The key step for methanol formation on neutral Nb_8 clusters is that CO must be molecularly adsorbed on the Nb_8 cluster surface. If CO were to dissociate rapidly on the clusters to form CNb_nO before collision with hydrogen molecules, recombination of carbon and oxygen atoms would not be possible, and transfer of hydrogen atoms to form methanol could not occur. Thus, the CO dissociation

Fig. 11. A potential energy surface profile for the reaction $Nb_8 + CO + 2H_2 \rightarrow Nb_8 + CH_3OH$. Energies are in eV and relative to the initial reactant energy of $Nb_8 + CO + 2H_2$. Energy levels are calculated by BPW91/LANL2DZ/6-311+G(2d, p). From Ref. [71].

Table 3
CO dissociation barriers and reaction rate constants on Nb_n cluster surface, as calculated by BPW91/LANL2DŽLANL2DŽ6-311+G(2d). Energies are in eV and relative to the initial energy ($Nb_n + CO$).

Clusters	Nb_nCO[a]	TS0[b]	k_n (s^{-1})[c]	t_n (s)[d]
Nb_3	1.99	0.88	3.18×10^{10}	3.15×10^{-11}
Nb_4	1.81	0.43	3.71×10^{8}	2.70×10^{-9}
Nb_7	1.66	0.57	5.41×10^{7}	1.85×10^{-8}
Nb_8	1.48	0.14	6.41×10^{4}	1.56×10^{-5}
Nb_{10}	1.23	…	…	…

Ref. [71].
[a] Association energy.
[b] Transition state energy for Nb_nCO to CNb_nO.
[c] Calculated reaction rate constant.
[d] Transition state lifetime $t_n = 1/k_n$.

rate constant on the clusters is an essential parameter for the formation of methanol. The CO dissociation rate constants on Nb_3, Nb_4, and Nb_7 are likewise calculated as 3.18×10^{10}, 3.71×10^{8}, and 5.41×10^{7} s^{-1}, respectively, as listed in Table 3. Note that the rate constants k_3, k_4, and k_7 are much larger than k_8, which suggests that CO is rapidly dissociated within nanoseconds to CNb_nO on the Nb_n clusters ($n = 3$, 4, and 7) prior to collision with H_2/He. Thus, methanol formation is suppressed on Nb_n ($n \neq 8$) cluster surfaces as CO can dissociate on these clusters before the Nb_nCO intermediate can adsorb a hydrogen molecule. For larger clusters than Nb_8, the H transfer barriers may be too high and the CO adsorption energy too low to support methanol formation.

3.2.2. $V_mO_n + NO + NH_3$

The second example for bond activation and chemisorption is selective catalytic reduction (SCR) of nitric oxide by ammonia. This reaction over V_2O_5/TiO_2 based catalysts is the most advanced and widely used technology capable of reducing NO_x emissions to the low levels mandated in many areas of the world [163]. The overall catalytically promoted reactions are

$$6NO + 4NH_3 \rightarrow 5N_2 + 6H_2O, \tag{12a}$$

$$6NO_2 + 8NH_3 \rightarrow 7N_2 + 12H_2O, \text{ etc.} \tag{12b}$$

The reactivity of neutral vanadium and tantalum oxide clusters toward NO, NH_3, and an NO/NH_3 mixture has been explored experimentally and theoretically [164]. An abundance of association products for the reaction $V_mO_n + NH_3$ and only a few association products (VO_3NO and V_2O_5NO) for the reaction $V_mO_n + NO$ are observed. DFT calculations suggest that the association energy for NH_3 and V_mO_n (~3 eV) is in general larger than the association energy for NO and V_mO_n (~1 eV). These results taken together indicate that the interaction of V_mO_n with ammonia is much stronger than the interaction of V_mO_n with NO. Therefore, in a competitive environment, ammonia will be preferentially chemisorbed on a catalytic vanadium oxide cluster as the first step, rather than NO in the SCR process. The N–H bond of the chemisorbed NH_3 on a V atom of an oxygen rich cluster (e.g., VO_3 and V_2O_5) can be activated, and one hydrogen easily transfers to an O atom to form VOH and a H_2NV moieties within the V_mO_n cluster. The reaction of the NH_2 moiety of chemisorbed NH_3 and NO on a VO_3 cluster is shown in Fig. 12.

The reaction starts, following formation of $HOVO_2NH_2$, by introducing an NO molecule to form intermediate **1**, in which N from the NH_2 radical and N from the NO radical are weakly bound. Via transition structure **1/2**, a lowest energy intermediate **2** with two moieties, $ONNH_2$ and $HOVO_2$, is formed. The two moieties can then separate and proceed to product **3** consisting of two separate molecules. A free $ONNH_2$ molecule now is produced. Final production of $N_2 + H_2O$ from $ONNH_2$ involves a complex mechanism that has no barrier with respect to the final product formation reaction $ONNH_2 \rightarrow N_2 + H_2O$ [163,165,166]. For the

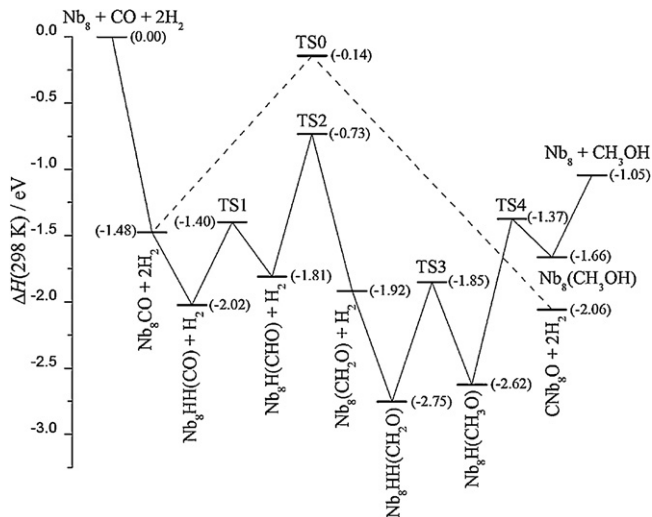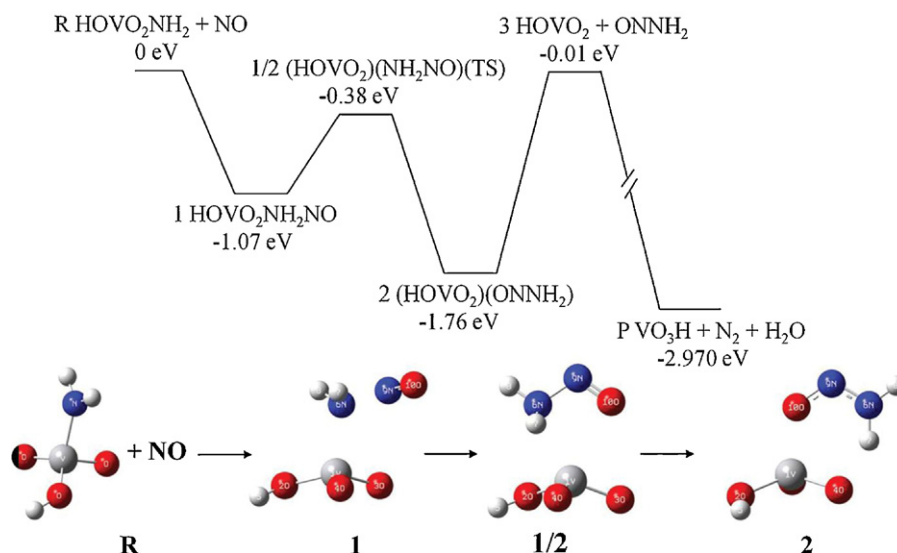**Fig. 12.** DFT calculated potential energy surface for the $VO_3 + NO:NH_3$ reaction. Structures are the optimized geometries of the reaction intermediates and transition states. Relative energies are in eV.
Adapted from Ref. [164].

Ta species (TaO_3), reactions with $NH_3 + NO$, a very stable lowest energy intermediate $(HO)_2TaOONNH$ forms via hydrogen transfer. Generation of product $H_2TaO_3 + ONNH$ is thermodynamically and kinetically unavailable for the tantalum oxide reaction, which suggest that the reaction should not proceed to form the final products $N_2 + H_2O$. Overall, the results suggest that vanadium oxide should make a better catalyst for the SCR of NO with NH_3 than tantalum oxide.

3.2.3. $V_mS_n + C_2H_4 + H_2$

The third example of chemisorptions and bond activation catalysis is hydrogenation reactions of C_2H_4 with H_2 on neutral vanadium sulfide clusters, again investigated by TOFMS employing 118 nm single photon ionization and DFT calculations [73]. The observed reactions of V_mS_n clusters with C_2H_4 and H_2 generate a new cluster series: the adduct of both C_2H_4 and H_x to form the products $VS_{1-3}C_2H_x$, $V_2S_{1-5}C_2H_x$ ($x = 5, 6$). The hydrogenation reactions of C_2H_4 with H_2 are thermodynamically available on V_mS_n ($m = 1, n = 1–3$; $m = 2, n = 1–5$) clusters. The V atoms are the active sites for these V_mS_n clusters for chemisorptions of a C_2H_4 molecule as the first step in the hydrogenation reactions of C_2H_4 with H_2. Two types of association products for ethylene on active V sites of catalytic V_mS_n clusters are determined by DFT calculations (Fig. 13). The C_2H_4 can connect with the active V atom through its π orbital or form a σ bond with active V atoms. Although the binding energy of ethylene with V_mS_n clusters of a σ type (1.37–1.76 eV) is larger than that of a π type (0.67–1.09 eV), the difference of binding energy between π and σ types does not generate an important effect on the continuing hydrogenation reaction of ethylene.

Both π and σ associated ethylene can be hydrogenated with H_2 on catalytic V_mS_n clusters. The PES along the reaction coordinate for hydrogenation reactions of C_2H_4 with H_2 on the V_2S_2 clusters is shown in Fig. 14 as an example. The H_2 molecule is predicted to be adsorbed on the V site of $V_2S_2C_2H_4$ cluster, and dissociates to form $-VH$ and/or $-SH$ groups. The H–H bond of the H_2 molecule can also rupture directly on two adjacent S sites: this process forms $-SH$ groups. The reaction mechanism on the VS_3 cluster is different: the hydrogen molecule attaches to $VS_3C_2H_4$, and the H–H bond ruptures with a small barrier ($\sim$0.1 eV) to form two $-SH$ groups on the S active sites directly. A higher barrier implies the reaction will be slower and thus the related product signal is weaker.

From the experimental observations, the intensity ratio of mass peak $V_2S_2C_2H_4HH$ to $V_2S_2C_2H_4$ is about 32%, whereas the ratio for $VS_3C_2H_4HH$ to $VS_3C_2H_4$ is only about 9%. The deduction from the calculation results is in good agreement with the experimental results.

The activation of the H_2 molecule on the $V_mS_nC_2H_4$ cluster series is associated with unpaired electron density localized on different active sites. Sufficient unpaired spin density on V or S atoms is responsible for the adsorption and dissociation of H_2. The H atoms of the $-VH$ and $-SH$ groups then transfer step by step to the C_2H_4, which is adsorbed on the catalytic V_mS_n cluster. The ethane molecule can be formed through an ethyl intermediate species which bonds to an active V site, and desorbs to the gas phase with the catalytic V_mS_n cluster unchanged.

3.2.4. Others

Some other theoretical and experimental investigations for bond activation and chemisorption reactions on the metal containing clusters are also in progress in our group. Only a brief introduction of these studies will be presented here. NH_3 generation through reaction of clusters Co_mN with H_2 is investigated employing TOFMS and 193 nm SPI. Clusters Co_mN ($m = 7, 8, 9$) have high reactivity with H_2 for the ammonia generation. Multiple molecular collision reactions are observed in some previous studies: for reactions of neutral iron oxide clusters with methanol [69], products $(CH_2O)FeOH$ and $FeOH$ are both observed due to multiple molecule collision reactions (e.g., $2FeO + CH_3OH$); series products $V_mS_nC_2H_5$ and V_mS_nH are observed through multiple molecule collision reactions in the reaction of V_mS_n clusters with C_2H_4 and H_2 [73]; and odd hydrogen atom numbers on the cluster system $M_mC_nH_x$ (M = Al, Be, Mg) [40,74], are also observed. Thus, an odd number of hydrogen atoms in Co_mNH_3 ($m = 7, 8, 9$) probably comes from the hydrogen molecule activation reaction on two cobalt containing clusters: for example, $2Co_7N + H_2 \rightarrow 2Co_7NH$. Theoretical DFT calculations are performed to explore the potential energy surface for the reaction $Co_7N + 3/2H_2 \rightarrow Co_7NH_3$. Both experimental observations and theoretical calculations suggest that the reaction of ammonia generation requires two active sites, and hydrogen activation on these two active sites is the key step by which to form NH_3. This seems to be a general mechanism for the catalytic generation of odd hydrogen containing molecules and clusters.
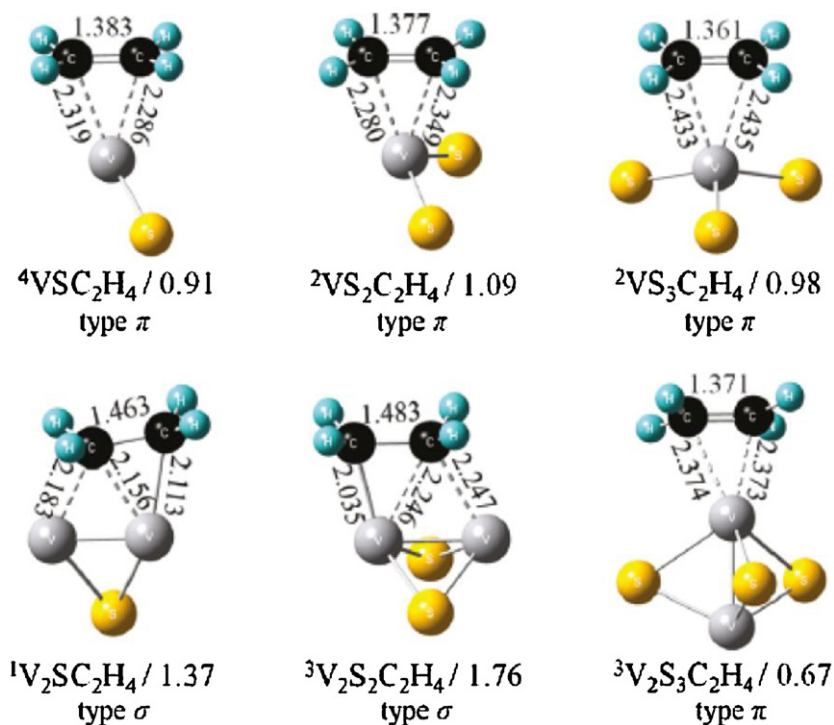
Fig. 13. DFT optimized geometries of association products $^MV_{1,2}S_{1-3}C_2H_4$. Two types of geometry configurations (π and σ) are presented. For each cluster, only the lowest energy structure with spin multiplicity (M) is listed. The value in eV below the geometry is the zero-point vibrational energy corrected binding energies (the BSSE corrections are ignored as less than 10%). The C—C and V—C bond length values in Å are given. From Ref. [73].

Reactions of neutral iron sulfide and hydrogen containing clusters ($Fe_mS_nH_x$, $m = 1–4$, $n = 2–6$, $x = 0–4$) with CO, C_2H_4, C_3H_6 and O_2 are investigated by TOFMS employing 118 nm SPI. The new products $Fe_3S_2O_{0,1}H_{0,1}$ and $Fe_4S_3O_{0,1}H_{0,1}$ are observed for reaction of $Fe_mS_nH_x$ clusters with O_2. O_2 can be activated on the $Fe_3S_3H_{0,1}$ and $Fe_4S_4H_{0,1}$ clusters at low temperature to form SO and SO_2 during the reactions. For the reaction of $Fe_mS_nH_x$ clusters with CO, C_2H_4 and C_3H_6, only the association products $Fe_2S_2(SH)_{0,1}X$ and $Fe_4S_4(SH)_{0,1}X$ (X = CO, C_2H_4, C_3H_6) are obtained, which suggests that the $Fe_2S_2(SH)_{0,1}$ and $Fe_4S_4(SH)_{0,1}$ clusters have high activity for chemisorption with CO, C_2H_4, C_3H_6. Theoretical calculations (in progress) suggest the Fe atoms in these clusters are the active sites for chemisorptions of the X molecule.

4. Understanding of the condensed phase catalytic process at a molecular level

Gas phase catalytic metal and metal compound clusters composed of limited numbers of atoms that are fully accessible by both experiment and theory are excellent model and functional systems with which to investigate the intrinsic reaction mechanisms for condensed phase catalytic processes [15,16]. Studies of small molecule reactions catalyzed by neutral metal containing clusters in the gas phase can aid in the understanding of the related condensed phase catalysis reaction at a molecular level. One can also concluded on the basis of numerous studies [18,19,167–170] that the interplay between cluster physics and surface chemistry is a promising strategy by which to uncover "mechanisms of elementary steps in nanocatalysis" [171]. On the basis of experimental and calculational results presented above, catalytic cycles for condensed phase reactions can be proposed. In this section, two systems will be described in detail as examples, and both deal with the catalysis of reaction (CO + 1/2O$_2$ → CO$_2$) by neutral cobalt oxide and iron oxide clusters. Hence we emphasize catalytic neutral metal

oxide clusters, as the study brings into focus and represents the active sites that exist on a catalyst surface.

A redox mechanism by which CO is oxidized to CO$_2$ and the reduced catalyst is oxidized by gas phase O$_2$ has been suggested for CO oxidation over a cobalt oxide catalyst [68,138,172–174]. The proposed mechanism is based on the Mars van Krevelen mechanism [175]. This mechanism includes a lattice atom transferred to generate the oxidized product and its replacement in the lattice by addition of a gas phase molecule or atom: the overall mechanism
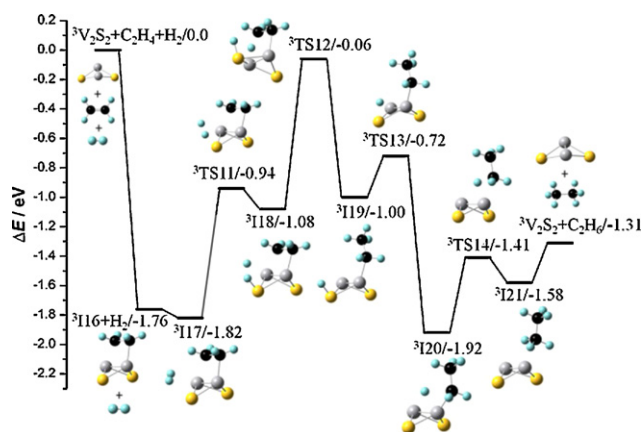
Fig. 14. Reaction pathway for $^3V_2S_2 + C_2H_4 + H_2 \rightarrow {}^3V_2S_2 + C_2H_6$ calculated at the BPW91/TZVP level. Energies, including ZPE corrections, are given in eV and are relative to the initial energy of the $^3V_2S_2 + C_2H_4 + H_2$ reactants. The reaction intermediates and transition states are denoted as ^MIn and ^MTSn, respectively, in which the superscript M indicates the spin multiplicity. V atoms are gray color, S atoms are yellow color, C atoms are black color, and H atoms are cyan color. (For interpretation of the references to color in this figure legend, the reader is referred to the web version of the article.) From Ref. [73].

Fig. 15. Proposed full catalytic cycle for CO oxidation to CO_2 on a cobalt oxide surface based on the calculations for the reaction of Co_3O_4 cluster with CO. From Ref. [68].

is clarified as a redox reaction. The most important information extracted from the CO oxidation on neutral cobalt oxide clusters for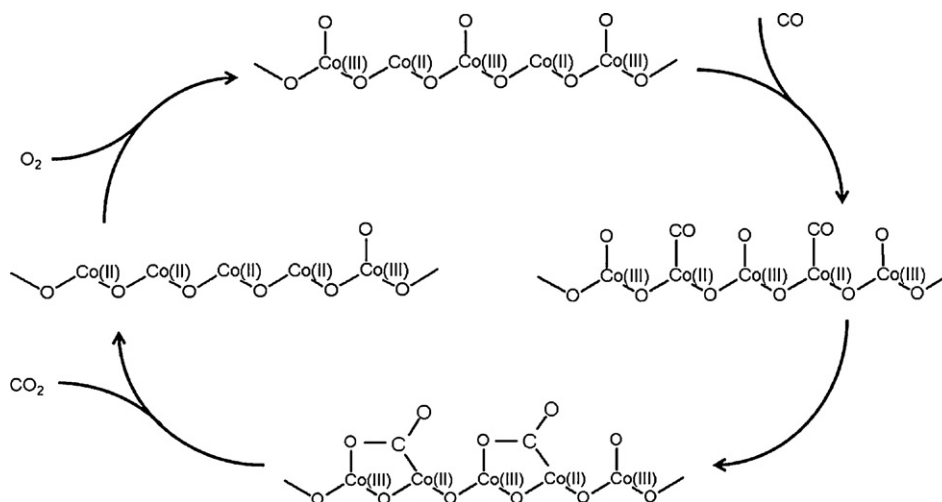 the condensed phase mechanism is the chemistry of the active sites on the cobalt oxide surface [68]. The proposed mechanism suggests that the CO molecule adsorbs on the Co(II) site and reacts with a neighboring oxygen atom, which is bound to an Co(III). The mechanism suggested from condensed phase studies cannot identify the oxidation state of the cobalt atom on which the CO is adsorbed, and DFT calculations for the condensed phase propose that CO is bound to Co(III) [68]. Since both Co(II) and Co(III) exist in the Co_3O_4 cluster, the catalytic cycle shown in Fig. 15 can model the Co_3O_4 catalyst surface behavior. As noted above, CO molecules are adsorbed on the Co(II) sites of the cobalt oxide catalyst surface, and CO_2 molecules are formed and dissociated from the surface by reaction of CO with the oxygen atom located on the Co(III) sites. After the reaction, Co(III) is reduced to Co(II).

The catalyst can be regenerated by reaction with O_2: O_2 molecules dissociate on the catalyst surface and Co(II) sites are re-oxidized to Co(III). The exposed Co(II) sites on the cobalt oxide catalyst surface are the active sites for the CO adsorption; however, pure Co_2O_3, for which only Co(III) sites exist, has no catalytic reactivity toward CO oxidation. The processes for CO oxidation and CO_2 desorption from the surface should be thermodynamically favorable, since the gas phase model reaction $CO + Co_3O_4 \rightarrow CO_2 + Co_3O_3$ is calculated as an exothermic reaction and has no reaction barrier [68]. Additionally, the CO oxidation reaction can occur at low temperature based on the condensed phase studies [137,138,172,176–180]. Regeneration of the catalyst is probably the rate limiting step for the whole catalytic cycle, because the catalyst must be heated to 250 °C or above to be re-oxidized [172].

The DFT calculations for O_2 adsorption and dissociation on neutral iron oxide clusters [69,140] indicate that oxidation of metal oxide clusters by O_2 probably involves high reaction barriers, since the strong O—O bond is broken through the oxidation processes. Generalizing this result, dissociation of O—O to form two Co—O bonds is energetically favorable, but with a high barrier. A parallel oxygen bridge is considered to be responsible for the high reactivity of the Co_3O_4 cluster for CO oxidation to CO_2. Oxygen atoms connected to the Co(III) sites and abstracted by CO (Fig. 15) can be suggested to have radical properties based on the gas phase cluster studies: they serve as the active sites, lower CO oxidation reaction barriers, and consequently accelerate CO oxidation to CO_2 in the condensed phase. This mechanism is based on gas phase cluster

studies; however, experimental data and theoretical calculations based on the nanocluster results are in general agreement with the condensed phase conclusions, and therefore help understand the heterogeneous catalytic reaction mechanism on real surfaces.

The redox mechanism, by which first CO is oxidized by the oxygen of the catalyst and second the reduced catalyst is oxidized by gas phase O_2, has also been suggested for CO oxidation over iron oxide catalysts [135,181]. Szegedi et al. found that iron oxide catalysts treated (oxidized) at 625 K with O_2 show very low reactivity, whereas the catalysts treated (reduced) above 773 K with H_2 show high reactivity [182]. The findings for the investigation of CO oxidation catalyzed by small neutral iron oxide clusters [140] can be used to rationalize interesting phenomena observed for the related condensed phase catalysis at a molecular level. The gas phase studies indicate that an iron center has to be provided for the initial intermediate (Fe_mO_nCO) formation through a carbon–iron interaction because direct CO_2 formation through the carbon–oxygen interaction is subject to high reaction barriers. For an oxygen-saturated surface treated with O_2 at high temperature, the CO has less chance to approach iron. The CO has a weaker interaction with an oxygen-saturated iron center than with an oxygen-unsaturated iron center, which may lead to a higher Fe—O bond activation barrier for an oxygen-saturated iron center than for an oxygen-unsaturated iron center. The Fe—O activation barriers are higher for the Fe—O bond on the iron atom connected to four O atoms, than for the one on the other iron atom connected to three O atoms (1.0–1.1 eV vs. 0.2–0.3 eV). On the other hand, for a reduced surface treated with H_2 at high temperature, more iron centers are present for O_xFe—CO complex formation. This point was also reported as a conclusion of ref [183] that the high density of Fe atoms on exposed {1 1 0} planes leads to high catalytic performance of the quasicubic α-Fe_2O_3 nanocrystals. Szegedi et al. found that the efficient condensed phase iron containing catalysts (treated with H_2/He at high temperature) have both ionic and metallic forms of iron. The metallic form of iron is suggested to play a role in CO activation through interaction of a metal ion, stabilized in the neighborhood of a supported metal nanocluster ("metal ion–metal nanocluster" ensemble site), with the lone pair of the oxygen atom of a chemisorbed CO molecule [182]. The study of CO oxidation catalyzed by small neutral iron oxide clusters [140] shows no evidence of interaction between the oxygen atom of CO and a metal ion (Fe^{3+}, Fe^{2+}) in the Fe_mO_n clusters. The mechanism of CO_2 formation over Fe_mO_n is quite simple: interaction of a lone pair of carbon with an iron atom and subsequent activation of an Fe—O bond that causes formation of another
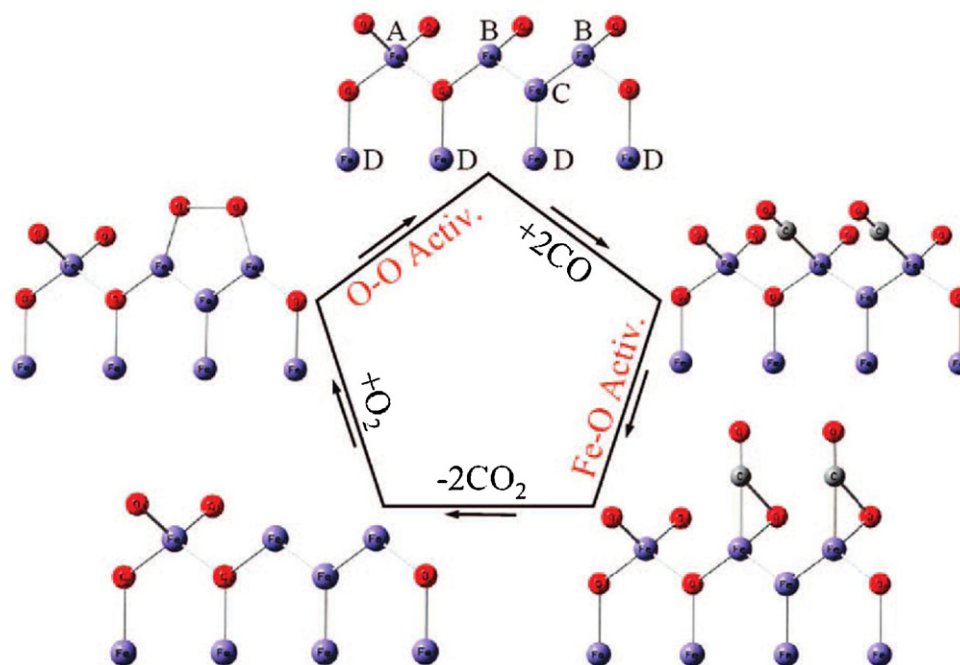
Fig. 16. Possible catalytic cycle for the CO oxidation by O_2 over iron oxide catalysts at the molecular level. A, B, and C mark different surface Fe atoms while D marks lattice Fe atoms that are underneath the surface.

From Ref. [140].

C=O bond. The Fe—O activation barrier is either negative or quite low (see Fig. 4). These cluster findings imply that the CO activation process suggested in Ref. [182] may not be required. Another important aspect of the redox mechanism deals with the O—O bond breaking (or O_2 activation) over the catalysts. In all of the three model catalytic cycles (Fig. 4) proposed, the process of the O—O bond breaking is the rate-limiting step. This suggests that efficient O_2 activation should be considered in practical catalysis.

The molecular level mechanism for CO oxidation with O_2, catalyzed by iron oxides is displayed in Fig. 16 [140]. Metallic (C), cationic (B), and over oxidized (A) surface Fe atoms (or sites) may be present in iron oxide catalysts prepared by different procedures. The over oxidized site A is not very catalytic because Fe is covered by too many O atoms which prevent CO/Fe coordination. The cationic site B is reactive toward CO oxidation by coordinating CO through carbon–iron interaction and subsequent Fe—O activation. The metallic site C promotes O—O activation over sites B or BCB, and a site like BCB should be very catalytic for the CO oxidation by O_2. This discussion, in particular, emphasizes the strong relationship between the detailed catalytic mechanism generated by means of gas phase cluster theory and experiment and the condensed phase parallel heterogeneous catalytic process.

5. Conclusions

This review has demonstrated that 193 nm, 118 nm, and 46.9 nm laser radiation, single photon ionization (SPI), coupled with time-of-flight mass spectrometry (TOFMS) can be successfully employed to investigate neutral metal, metal oxide/carbide/sulfide cluster distributions, reactivity, and chemistry in the gas phase. Density functional theory calculations for these systems enable exploration of the geometric and electronic structures of clusters and determination of reaction intermediates and transition states, as well as reaction mechanisms by comparing the results of theoretical calculations and experimental observations. These reaction mechanisms can then be employed to suggest full catalytic cycles for condensed phase reactivity and processes.

Oxidation–reduction reactions are an important category of chemical reactivity of neutral metal oxide clusters. The reactivity of metal oxide clusters with small gas phase molecules, such as CO, SO_2, and hydrocarbons, is associated with the oxygen-rich or -deficient nature of the cluster, bond enthalpy of the cluster, and cluster spin state and unpaired spin density.

Generally, oxygen-rich metal oxide clusters have high oxidation activity for oxidation reactions of small gas phase molecules. The oxygen that is bonded to a high oxidation state metal can be considered as reactive oxygen. The type of metal can influence activity of the reactive oxygen; however, the activity of an oxygen-rich metal oxide cluster toward small gas phase molecule oxidation is also driven by (1) smaller bond enthalpy of oxygen-rich metal oxide cluster (M—O) than that of the small molecule and (2) negative or very small overall oxidation reaction barrier (relative to initial energy of the reactants).

An oxidizing gas molecule, such as O_2, can oxidize an oxygen-deficient metal oxide cluster, due to its low oxidation state metal reactive center. Usually, the O—O bond (O_2) activation (or breaking) is the pivotal step for an oxygen-deficient metal oxide cluster oxidation reaction, and this process is subject to high reaction barrier.

On the basis of these general reaction mechanisms, the findings for the investigation of redox reactions catalyzed by neutral metal oxide clusters can be used to rationalize interesting phenomena observed for the related metal oxide condensed phase catalysis at a molecular level. On metal oxide condensed phase catalysts surface, the exposed low oxidation state metal sites are the active sites for reactant adsorption. The reactant molecules are easily adsorbed on the low oxidation state metal site and then react with neighboring oxygen atoms, which are bound to the high oxidation state metal. After reaction, the high oxidation state metal site is reduced to a low oxidation state metal site. The catalyst can be regenerated by reaction with O_2: O_2 molecules dissociate on the catalyst surface and low oxidation state metal sites are re-oxidized to a high oxidation state. Additionally, a reduced site can interact with an oxidized site and the two can react to regenerate the original catalytic site distribution. Regeneration of the catalyst is probably the rate limiting

step for the whole catalytic cycle due to reaction barrier and site mobility, so usually the catalyst needs to be heated. A suitable ratio and rational distribution of the high and low oxidation state metal sites on catalyst surfaces and fascile catalyst regeneration processes are suggested to be helpful to improve the efficiency of the metal oxide catalyst for oxidation–reduction catalysis. The reactions that lead to these generalizations are the following.

(1) SO_2 to SO conversion occurs for oxygen-poor vanadium oxide clusters and SO_2 to SO_3 conversion occurs for oxygen-rich vanadium oxide clusters. The profusion of reactant species, reaction intermediates and transition states, and even mechanisms for the conversion of SO_2 to SO_3 may be major reasons that vanadium oxide is an excellent oxidation/reduction catalyst for the reaction.

(2) FeO_2 and FeO_3 neutral clusters are reactive toward CO, whereas Fe_2O_4, Fe_2O_5 and FeO are not reactive. The reaction is driven by additional C=O bond formation which is facile due to favorable thermodynamics: CO_2 (O—CO) bond enthalpy (5.54 eV) is higher than those of FeO_{1-3} and $Fe_2O_{4,5}$ (2.93–4.29 eV).

(3) The Co_3O_4 cluster also has the highest reactivity for any Co_mO_n reactions with CO. This reactivity is associated with appropriate Co(III) concentration in the cobalt oxide clusters. CO molecules can be adsorbed on the Co(II) sites of the cobalt oxide catalyst surface, and CO_2 molecules are formed and dissociated from the surface by reaction of CO with the oxygen atom located on the Co(III) sites.

Another important type or class of catalytic reaction can be generalized as activation and transfer. Such a catalytic process occurs through reactant bond activation (barrier lowering) on a catalyst surface for which the catalyst simply activates (lower barriers) a relevant part of the reagent sufficiently and transfers the reactive fragment to a second molecule trapped at the catalyst surface. For this kind of bond activation catalysis reaction on metal and metal oxide/sulfide clusters in gas phase, the reaction is initiated by the adsorption of reactant molecules on the active metal sites of clusters.

The bond activation of the adsorbed reactant molecule is an essential step of the reaction, then the products dissociate from the cluster, and the structure and catalytic activity of the cluster does not change. High association energy between reactant molecules and clusters prevents dissociation of reactant molecules from active clusters and makes the continued bond activation of the reactant molecule possible. Lower activation energy (barriers) of the associated molecule relative to the association energy makes the reaction more facile on the active cluster. The catalytic activity of metal and metal oxide/sulfide clusters for bond activation catalysis is dependent up on the association and activation capabilities of the clusters with regard to the reactant molecules: this suggests that strong interaction of gas phase reactant molecules with a catalyst surface and low activation barriers for reactants on the catalyst surface are important features for designing metal and metal oxide/sulfide catalysts and improving their catalytic reactivity for a bond-activation catalysis mechanism. Nonetheless, the product must not be bound so tightly that it cannot be released from the catalyst with the remaining system reaction enthalpy. The balance between reactant-catalyst binding product release, and reaction enthalpy is thereby delicate.

Examples presented in this review that fall into this category are the following:

(1) During catalysis reactions of $CO + 2H_2 \rightarrow CH_3OH$ on pure metal clusters (V_n, Nb_n, and Ta_n), a special cluster Nb_8 is found that has high catalytic activity due to its higher association energy with CO and H_2, lower H—H bond activation, and lower hydrogen transfer barriers, compared to those on other types and sizes of metal clusters. Thus, Nb_8 can be considered a special site for catalytic activity for the reaction of CO and H_2 to generate methanol, due to its finely tuned, and delicately balanced, values of barriers and adsorption energies.

(2) For the selective catalytic reduction (SCR) of NO by NH_3, the V metal sites are the active sites for oxygen-rich clusters to attach NO and NH_3. The reaction barrier is lower on oxygen-rich V_mO_n clusters, compared with that on oxygen-rich Ta_mO_n clusters. Vanadium oxide is suggested to be a better catalyst for the SCR of NO with NH_3 than tantalum oxide, because complexes of NO and NH_3 formed at an oxygen-rich V_mO_n site can more easily follow the reaction path toward end products $N_2 + H_2O$. The addition of NH_3 on the cluster as a first step is also important for the overall adsorption and oxidation/reduction processes.

(3) Reactions of $C_2H_4 + H_2 \rightarrow C_2H_6$ are thermodynamically available on V_mS_n ($n \leq 2m+1$) clusters, not on V_mS_n ($n > 2m+1$) clusters. V atoms are active sites for the attachment of the C_2H_4 molecule. A higher H—H bond (H_2) activation barrier is responsible for the lower intensity of hydrogenation products (e.g., C_2H_6) observed on VS_3 relative to that on other catalytic VS_n clusters, such as on VS_2.

Overall, experimental and theoretical studies shown here provide unique insights into: (1) how the fundamental reactivity of neutral metal and metal compound clusters can be influenced by the type of metal, the oxygen-rich or -deficient nature of the cluster, bond enthalpy of cluster, electronic structure of cluster, and spin state and unpaired spin density of the cluster and (2) how the application of gas phase neutral metal cluster chemistry is instructive in the understanding of important fundamental aspects of practical catalysis in the condensed phase. These gas phase data and mechanisms can be used to rationalize and understand reactivity and mechanism in related condensed phase catalytic reaction at a molecular level.

A number of areas within cluster research can be identified as possible directions for future effort: (1) discovery of new catalytic systems for condensed phase application through gas phase cluster chemistry; (2) studies of mixed metal clusters to elucidate the nature of supported catalyst systems and chemistry; (3) detailed investigation of the different nature of neutral, cation, and anion chemistry and how these different chemistries relate to condensed phase catalytic behavior; and (4) direct application of very small clusters and molecules for in situ catalytic systems and processes.

References

[1] D.F. Shriver, P.W. Atkins, C.H. Langford, Inorganic Chemistry, O.U. Press, Oxford, 1994.
[2] G.A. Somorjai, Introduction to Surface Chemistry and Catalysis, Wiley, New York, 1994.
[3] J.L.G. Fierro, Metal Oxides Chemistry and Applications, Taylor & Francis, London, 2006.
[4] R.A.J. O'Hair, A.K. Vrkic, P.F. James, Journal of the American Chemical Society 126 (2004) 12173–12183.
[5] T. Waters, R.A.J. O'Hair, A.G. Wedd, Journal of the American Chemical Society 125 (2003) 3384–3396.
[6] A.T. Bell, Science 299 (2003) 1688–1691.
[7] B.H. Cornils, W.A. Herrmann, Applied Homogeneous Catalysis with Organometallic Compounds, VCH, Weinheim, 1996.

[8] M.A. Barteau, Chemical Reviews 96 (1996) 1413–1430.
[9] C.L. Thomas, Catalytic Processes and Proven Catalysts, Academic Press, New York, 1970.
[10] D. Schröder, H. Schwarz, Angewandte Chemie International Edition in English 34 (1995) 1973–1995.
[11] D.W. Goodman, Journal of Catalysis 216 (2003) 213–222.
[12] G.A. Somorjai, Journal of Physical Chemistry B 106 (2002) 9201–9213.
[13] T. Zambelli, J. Wintterlin, J. Trost, G. Ertl, Science 273 (1996) 1688–1690.
[14] J.M. Thomas, R. Raja, Topics in Catalysis 40 (2006) 3–17.
[15] E.L. Muetterties, Science 196 (1977) 839–848.
[16] P. Jena, A.W. Castleman, Proceedings of the National Academy of Sciences of the United States of America 103 (2006) 10560–10569.
[17] W.T. Wallace, R.L. Whetten, Journal of the American Chemical Society 124 (2002) 7499–7505.
[18] J. Hagen, L.D. Socaciu, M. Elijazyfer, U. Heiz, T.M. Bernhardt, L. Woste, Physical Chemistry Chemical Physics 4 (2002) 1707–1709.
[19] I. Balteanu, O.P. Balaj, B.S. Fox, M.K. Beyer, Z. Bastl, V.E. Bondybey, Physical Chemistry Chemical Physics 5 (2003) 1213–1218.
[20] W. Huang, H.J. Zhai, L.S. Wang, Journal of the American Chemical Society 132 (2010) 4344–4351.
[21] J.H. Futrell, Gaseous Ion Chemistry and Mass Spectrometry, Wiley, New York, 1986.
[22] K. Eller, H. Schwarz, Chemical Reviews 91 (1991) 1121–1177.
[23] C.A. Schalley, Modern Mass Spectrometry: Top. Curr. Chem., vol. 225, Springer, Berlin, 2003.
[24] J.H. Gross, Mass Spectrometry, Springer, Berlin, 2004.
[25] M.B. Knickelbein, Annual Review of Physical Chemistry 50 (1999) 79–115.
[26] P.B. Armentrout, Annual Review of Physical Chemistry 52 (2001) 423–461.
[27] T.G. Dietz, M.A. Duncan, D.E. Powers, R.E. Smalley, Journal of Chemical Physics 74 (1981) 6511–6512.
[28] M.E. Geusic, M.D. Morse, S.C. Obrien, R.E. Smalley, Review of Scientific Instruments 56 (1985) 2123–2130.
[29] M.D. Morse, M.E. Geusic, J.R. Heath, R.E. Smalley, Journal of Chemical Physics 83 (1985) 2293–2304.
[30] R.A.J. O'Hair, G.N. Khairallah, Journal of Cluster Science 15 (2004) 331–363.
[31] M. Foltin, G.J. Stueber, E.R. Bernstein, Journal of Chemical Physics 109 (1998) 4342–4360.
[32] M. Foltin, G.J. Stueber, E.R. Bernstein, Journal of Chemical Physics 111 (1999) 9577–9586.
[33] M. Foltin, G.J. Stueber, E.R. Bernstein, Journal of Chemical Physics 114 (2001) 8971–8989.
[34] S.G. He, Y. Xie, Y.Q. Guo, E.R. Bernstein, Journal of Chemical Physics 126 (2007) 194315/1–194315/9.
[35] F. Dong, S. Heinbuch, S.G. He, Y. Xie, J.J. Rocca, E.R. Bernstein, Journal of Chemical Physics 125 (2006) 164318/1–164318/8.
[36] Y. Matsuda, E.R. Bernstein, Journal of Physical Chemistry A 109 (2005) 314–319.
[37] D.N. Shin, Y. Matsuda, E.R. Bernstein, Journal of Chemical Physics 120 (2004) 4157–4164.
[38] D.N. Shin, Y. Matsuda, E.R. Bernstein, Journal of Chemical Physics 120 (2004) 4150–4156.
[39] F. Dong, S. Heinbuch, E.R. Bernstein, J.J. Rocca, X-ray Lasers 2006, Proceedings, vol. 115, 2007, pp. 463–469.
[40] F. Dong, S. Heinbuch, Y. Xie, J.J. Rocca, E.R. Bernstein, Physical Chemistry Chemical Physics 12 (2010) 2569–2581.
[41] M.M. Kappes, R.H. Staley, Journal of the American Chemical Society 103 (1981) 1286–1287.
[42] V. Baranov, G. Javahery, A.C. Hopkinson, D.K. Bohme, Journal of the American Chemical Society 117 (1995) 12801–12809.
[43] M. Brönstrup, D. Schröder, I. Kretzschmar, H. Schwarz, J.N. Harvey, Journal of the American Chemical Society 123 (2001) 142–147.
[44] V. Blagojevic, M.J.Y. Jarvis, E. Flaim, G.K. Koyanagi, V.V. Lavrov, D.K. Bohme, Angewandte Chemie International Edition 42 (2003) 4923–4927.
[45] V. Blagojevic, G. Orlova, D.K. Bohme, Journal of the American Chemical Society 127 (2005) 3545–3555.
[46] L.D. Socaciu, J. Hagen, T.M. Bernhardt, L. Woste, U. Heiz, H. Hakkinen, U. Landman, Journal of the American Chemical Society 125 (2003) 10437–10445.
[47] O.P. Balaj, I. Balteanu, T.T.J. Rossteuscher, M.K. Beyer, V.E. Bondybey, Angewandte Chemie International Edition 43 (2004) 6519–6522.
[48] B. Chiavarino, M.E. Crestoni, S. Fornarini, Chemistry: A European Journal 8 (2002) 2740–2746.
[49] R.B. Wyrwas, C.C. Jarrold, Journal of the American Chemical Society 128 (2006) 13688–13689.
[50] X.L. Ding, X.N. Wu, Y.X. Zhao, S.G. He, Accounts of Chemical Research 45 (2012) 382–390.
[51] Y.X. Zhao, X.N. Wu, J.B. Ma, S.G. He, X.L. Ding, Physical Chemistry Chemical Physics 13 (2011) 1925–1938.
[52] D.K. Böhme, H. Schwarz, Angewandte Chemie International Edition 44 (2005) 2336–2354.
[53] D. Schröder, H. Schwarz, Proceedings of the National Academy of Sciences of the United States of America 105 (2008) 18114–18119.
[54] A.W. Castleman, Catalysis Letters 141 (2011) 1243–1253.
[55] J. Roithová, D. Schröder, Chemical Reviews 110 (2010) 1170–1211.
[56] E.F. Fialko, A.V. Kikhtenko, V.B. Goncharov, K.I. Zamaraev, Journal of Physical Chemistry A 101 (1997) 8607–8613.
[57] K.A. Zemski, D.R. Justes, A.W. Castleman, Journal of Physical Chemistry B 106 (2002) 6136–6148.
[58] D.R. Justes, R. Mitric, N.A. Moore, V. Bonacic-Koutecky, A.W. Castleman, Journal of the American Chemical Society 125 (2003) 6289–6299.
[59] D.R. Justes, N.A. Moore, A.W. Castleman, Journal of Physical Chemistry B 108 (2004) 3855–3862.
[60] M.L. Kimble, A.W. Castleman, R. Mitric, C. Burgel, V. Bonacic-Koutecky, Journal of the American Chemical Society 126 (2004) 2526–2535.
[61] S. Feyel, D. Schröder, X. Rozanska, J. Sauer, H. Schwarz, Angewandte Chemie International Edition 45 (2006) 4677–4681.
[62] S. Feyel, J. Döbler, D. Schröder, J. Sauer, H. Schwarz, Angewandte Chemie International Edition 45 (2006) 4681–4685.
[63] L. Operti, R. Rabezzana, Mass Spectrometry Reviews 25 (2006) 483–513.
[64] J.M.C. Plane, R.J. Rollason, Physical Chemistry Chemical Physics 1 (1999) 1843–1849.
[65] R.J. Rollason, J.M.C. Plane, Physical Chemistry Chemical Physics 2 (2000) 2335–2343.
[66] G.J. Wang, Y. Gong, M.H. Chen, M.F. Zhou, Journal of the American Chemical Society 128 (2006) 5974–5980.
[67] Y. Matsuda, E.R. Bernstein, Journal of Physical Chemistry A 109 (2005) 3803–3811.
[68] Y. Xie, F. Dong, S. Heinbuch, J.J. Rocca, E.R. Bernstein, Physical Chemistry Chemical Physics 12 (2010) 947–959.
[69] Y. Xie, F. Dong, S. Heinbuch, J.J. Rocca, E.R. Bernstein, Journal of Chemical Physics 130 (2009) 114306/1–114306/11.
[70] F. Dong, S. Heinbuch, Y. Xie, E.R. Bernstein, J.J. Rocca, Z.C. Wang, X.L. Ding, S.G. He, Journal of the American Chemical Society 131 (2009) 1057–1066.
[71] Y. Xie, S.G. He, F. Dong, E.R. Bernstein, Journal of Chemical Physics 128 (2008) 044306/1–044306/9.
[72] S.G. He, Y. Xie, F. Dong, S. Heinbuch, E. Jakubikova, J.J. Rocca, E.R. Bernstein, Journal of Physical Chemistry A 112 (2008) 11067–11077.
[73] S. Yin, Y. Xie, E.R. Bernstein, Journal of Physical Chemistry A 115 (2011) 10266–10275.
[74] F. Dong, Y. Xie, E.R. Bernstein, Journal of Chemical Physics 135 (2011) 054307/1–054307/6.
[75] Y. Matsuda, D.N. Shin, E.R. Bernstein, Journal of Chemical Physics 120 (2004) 4142–4149.
[76] E.L. Muetterties, T.N. Rhodin, E. Band, C.F. Brucker, W.R. Pretzer, Chemical Reviews 79 (1979) 91–137.
[77] G. Ertl, H.J. Freund, Physics Today 52 (1999) 32–38.
[78] R. Hilbig, R. Wallenstein, IEEE Journal of Quantum Electronics 17 (1981) 1566–1573.
[79] R.H. Page, R.J. Larkin, A.H. Kung, Y.R. Shen, Y.T. Lee, Review of Scientific Instruments 58 (1987) 1616–1620.
[80] M.P. McCann, C.H. Chen, M.G. Payne, Journal of Chemical Physics 89 (1988) 5429–5441.
[81] P.G. Strupp, A.L. Alstrin, R.V. Smilgys, S.R. Leone, Applied Optics 32 (1993) 842–846.
[82] K. Suto, Y. Sato, C.L. Reed, V. Skorokhodov, Y. Matsumi, M. Kawasaki, Journal of Physical Chemistry A 101 (1997) 1222–1226.
[83] K. Tonokura, T. Murasaki, M. Koshi, Chemical Physics Letters 319 (2000) 507–511.
[84] R.H. Lipson, S.S. Dimov, P. Wang, Y.J. Shi, D.M. Mao, X.K. Hu, J. Vanstone, Instrumentation Science & Technology 28 (2000) 85–118.
[85] Y.J. Shi, S. Consta, A.K. Das, B. Mallik, D. Lacey, R.H. Lipson, Journal of Chemical Physics 116 (2002) 6990–6999.
[86] F. Dong, S. Heinbuch, J.J. Rocca, E.R. Bernstein, Journal of Chemical Physics 124 (2006) 224319/1–224319/17.
[87] M.G. Bawendi, W.L. Wilson, L. Rothberg, P.J. Carroll, T.M. Jedju, M.L. Steigerwald, L.E. Brus, Physical Review Letters 65 (1990) 1623–1626.
[88] O.I. Micic, A.J. Nozik, E. Lifshitz, T. Rajh, O.G. Poluektov, M.C. Thurnauer, Journal of Physical Chemistry B 106 (2002) 4390–4395.
[89] R. Doolen, R. Laitinen, F. Parsapour, D.F. Kelley, Journal of Physical Chemistry B 102 (1998) 3906–3911.
[90] J.P. Wilcoxon, J.E. Martin, F. Parsapour, B. Wiedenman, D.F. Kelley, Journal of Chemical Physics 108 (1998) 9137–9143.
[91] Z.G. Zhang, H.G. Xu, X.Y. Kong, W.J. Zheng, Journal of Physical Chemistry A 115 (2011) 13–18.
[92] A.N. Alexandrova, A.I. Boldyrev, X.A. Li, H.W. Sarkas, J.H. Hendricks, S.T. Arnold, K.H. Bowen, Journal of Chemical Physics 134 (2011) 044322/1–044322/8.
[93] K. Majer, M. Lei, C. Hock, B. von Issendorff, A. Aguado, Journal of Chemical Physics 131 (2009) 204313/1–204313/10.
[94] X. Li, S. Eustis, K.H. Bowen, A.K. Kandalam, P. Jena, Journal of Chemical Physics 129 (2008) 074313/1–074313/11.
[95] H. Hakkinen, B. Yoon, U. Landman, X. Li, H.J. Zhai, L.S. Wang, Journal of Physical Chemistry A 107 (2003) 6168–6175.
[96] M. Citir, G. Altinay, G. Austein-Miller, R.B. Metz, Journal of Physical Chemistry A 114 (2010) 11322–11329.
[97] G. Santambrogio, M. Brummer, L. Woste, J. Dobler, M. Sierka, J. Sauer, G. Meijer, K.R. Asmis, Physical Chemistry Chemical Physics 10 (2008) 3992–4005.
[98] E. Jakubikova, A.K. Rappe, E.R. Bernstein, Journal of Physical Chemistry A 111 (2007) 12938–12943.
[99] W.Y. Kang, E.R. Bernstein, Bulletin of the Korean Chemical Society 26 (2005) 345–348.
[100] Y. Matsuda, D.N. Shin, E.R. Bernstein, Journal of Chemical Physics 120 (2004) 4165–4171.

[101] R. Nowak, J.A. Menapace, E.R. Bernstein, Journal of Chemical Physics 89 (1988) 1309–1321.
[102] T. Albaret, F. Finocchi, C. Noguera, Journal of Chemical Physics 113 (2000) 2238–2249.
[103] J.L. Persson, M. Andersson, L. Holmgren, T. Aklint, A. Rosen, Chemical Physics Letters 271 (1997) 61–66.
[104] V. Boutou, M.A. Lebeault, A.R. Allouche, F. Paulig, J. Viallon, C. Bordas, J. Chevaleyre, Journal of Chemical Physics 112 (2000) 6228–6236.
[105] B. Dai, L. Tian, J.L. Yang, Journal of Chemical Physics 120 (2004) 2746–2751.
[106] J.L.G. Fierro, Metal Oxides Chemistry and Applications, Taylor & Francis, Boca Raton, 2006.
[107] G. Ertl, H. Knözinger, J. Weitkamp, Handbook of Heterogeneous Catalysis, Wiley-VCH, Weinheim, 1997.
[108] F. Ogliaro, N. Harris, S. Cohen, M. Filatov, S.P. de Visser, S. Shaik, Journal of the American Chemical Society 122 (2000) 8977–8989.
[109] K.A. Zemski, D.R. Justes, R.C. Bell, A.W. Castleman, Journal of Physical Chemistry A 105 (2001) 4410–4417.
[110] M. Schlangen, D. Schröder, H. Schwarz, Angewandte Chemie International Edition 46 (2007) 1641–1644.
[111] B. de Bruin, P.H.M. Budzelaar, A.W. Gal, Angewandte Chemie International Edition 43 (2004) 4142–4157.
[112] M. Calatayud, B. Mguig, C. Minot, Surface Science Reports 55 (2004) 169–236.
[113] K.R. Asmis, M. Brummer, C. Kaposta, G. Santambrogio, G. von Helden, G. Meijer, K. Rademann, L. Woste, Physical Chemistry Chemical Physics 4 (2002) 1101–1104.
[114] I.T. Horvath, Encyclopedia of Catalysis, Wiley, New York, 2003.
[115] B.M. Weckhuysen, D.E. Keller, Catalysis Today 78 (2003) 25–46.
[116] J.L.G. Fierro, Metal Oxides, Taylor & Francis, London, 2006.
[117] E. Jakubikova, E.R. Bernstein, Journal of Physical Chemistry A 111 (2007) 13339–13346.
[118] J.P. Dunn, H.G. Stenger, I.E. Wachs, Catalysis Today 51 (1999) 301–318.
[119] J.P. Dunn, H.G. Stenger, I.E. Wachs, Catalysis Today 53 (1999) 543–556.
[120] I.E. Wachs, Catalysis Today 100 (2005) 79–94.
[121] M. Haruta, T. Tsubota, T. Kobayashi, H. Kageyama, M.J. Genet, B. Delmon, Journal of Catalysis 144 (1993) 175–192.
[122] S.S. Lee, C.Y. Fan, T.P. Wu, S.L. Anderson, Journal of the American Chemical Society 126 (2004) 5682–5683.
[123] S. Lee, C.Y. Fan, T.P. Wu, S.L. Anderson, Journal of Chemical Physics 123 (2005) 124710/1–124710/13.
[124] D.C. Meier, D.W. Goodman, Journal of the American Chemical Society 126 (2004) 1892–1899.
[125] T.V. Choudhary, D.W. Goodman, Applied Catalysis A: General 291 (2005) 32–36.
[126] T.V.W. Janssens, A. Carlsson, A. Puig-Molina, B.S. Clausen, Journal of Catalysis 240 (2006) 108–113.
[127] A.S.K. Hashmi, G.J. Hutchings, Angewandte Chemie International Edition 45 (2006) 7896–7936.
[128] B.K. Min, C.M. Friend, Chemical Reviews 107 (2007) 2709–2724.
[129] A.A. Herzing, C.J. Kiely, A.F. Carley, P. Landon, G.J. Hutchings, Science 321 (2008) 1331–1335.
[130] A. Fielicke, G. von Helden, G. Meijer, B. Simard, D.M. Rayner, Journal of Physical Chemistry B 109 (2005) 23935–23940.
[131] A. Fielicke, G. von Helden, G. Meijer, D.B. Pedersen, B. Simard, D.M. Rayner, Journal of Chemical Physics 124 (2006) 194305/1–194305/8.
[132] N. Veldeman, P. Lievens, M. Andersson, Journal of Physical Chemistry A 109 (2005) 11793–11801.
[133] A. Prestianni, A. Martorana, F. Labat, I. Ciofini, C. Adamo, Journal of Physical Chemistry B 110 (2006) 12240–12248.
[134] G.E. Johnson, N.M. Reilly, E.C. Tyo, A.W. Castleman, Journal of Physical Chemistry C 112 (2008) 9730–9736.
[135] M.A. Uddin, T. Komatsu, T. Yashima, Journal of Catalysis 146 (1994) 468–475.
[136] M.H. Khedr, K.S.A. Halim, M.I. Nasr, A.M. El-Mansy, Materials Science and Engineering A 430 (2006) 40–45.
[137] L.F. Liotta, M. Ousmane, G. Di Carlo, G. Pantaleo, G. Deganello, G. Marci, L. Retailleau, A. Giroir-Fendler, Applied Catalysis A: General 347 (2008) 81–88.
[138] M.J. Pollard, B.A. Weinstock, T.E. Bitterwolf, P.R. Griffiths, A.P. Newbery, J.B. Paine, Journal of Catalysis 254 (2008) 218–225.
[139] Y. Xie, F. Dong, E.R. Bernstein, Catalysis Today 177 (2011) 64–71.
[140] W. Xue, Z.C. Wang, S.G. He, Y. Xie, E.R. Bernstein, Journal of the American Chemical Society 130 (2008) 15879–15888.
[141] J.R. Wilson, G. Burgh, Energizing our Future: Rational Choices for the 21st Century, Wiley, Hoboken, NJ, 2008.
[142] G.A. Olah, A. Goeppert, G.K.S. Prakash, Beyond Oil and Gas: The Methanol Economy, Wiley-VCH, Weinheim, 2006.
[143] G.C. Chinchen, P.J. Denny, J.R. Jennings, M.S. Spencer, K.C. Waugh, Applied Catalysis 36 (1988) 1–65.
[144] X.M. Liu, G.Q. Lu, Z.F. Yan, J. Beltramini, Industrial and Engineering Chemistry Research 42 (2003) 6518–6530.
[145] A.P.V. Soares, M.F. Portela, Catalysis Reviews: Science and Engineering 47 (2005) 125–174.
[146] M.P. House, A.F. Carley, M. Bowker, Journal of Catalysis 252 (2007) 88–96.
[147] M. Engeser, D. Schröder, H. Schwarz, Chemistry: A European Journal 11 (2005) 5975–5987.
[148] M. Engeser, D. Schröder, H. Schwarz, European Journal of Inorganic Chemistry (2007) 2454–2464.
[149] S. Feyel, L. Scharfenberg, C. Daniel, H. Hartl, D. Schröder, H. Schwarz, Journal of Physical Chemistry A 111 (2007) 3278–3286.
[150] E.F. Fialko, A.V. Kikhtenko, V.B. Goncharov, Organometallics 17 (1998) 25–31.
[151] K. Yoshizawa, Y. Kagawa, Journal of Physical Chemistry A 104 (2000) 9347–9355.
[152] M.J. Louwerse, P. Vassilev, E.J. Baerends, Journal of Physical Chemistry A 112 (2008) 1000–1012.
[153] M.C. Oliveira, J. Marcalo, M.C. Vieira, M.A.A. Ferreira, International Journal of Mass Spectrometry 185 (1999) 825–835.
[154] P. Jackson, K.J. Fisher, G.D. Willett, Chemical Physics 262 (2000) 179–187.
[155] D. Schröder, R. Wesendrup, C.A. Schalley, W. Zummack, H. Schwarz, Helvetica Chimica Acta 79 (1996) 123–132.
[156] J.R. Valbert, J.G. Zajacek, D.I. Orenbuch, Encyclopedia of Chemical Processing and Design, Marcel Dekker, New York, 1993.
[157] C.L. Zhao, I.E. Wachs, Catalysis Today 118 (2006) 332–343.
[158] M. Ruszel, B. Grzybowska, M. Gasior, K. Samson, I. Gressel, J. Stoch, Catalysis Today 99 (2005) 151–159.
[159] F. Dong, S. Heinbuch, Y. Xie, J.J. Rocca, E.R. Bernstein, Z.C. Wang, K. Deng, S.G. He, Journal of the American Chemical Society 130 (2008) 1932–1943.
[160] Z.C. Wang, W. Xue, Y.P. Ma, X.L. Ding, S.G. He, F. Dong, S. Heinbuch, J.J. Rocca, E.R. Bernstein, Journal of Physical Chemistry A 112 (2008) 5984–5993.
[161] Y.P. Ma, X.L. Ding, Y.X. Zhao, S.G. He, ChemPhysChem: A European Journal of Chemical Physics and Physical Chemistry 11 (2010) 1718–1725.
[162] D.B. Pedersen, D.M. Rayner, B. Simard, M.A. Addicoat, M.A. Buntine, G.F. Metha, A. Fielicke, Journal of Physical Chemistry A 108 (2004) 964–970.
[163] S. Soyer, A. Uzun, S. Senkan, I. Onal, Catalysis Today 118 (2006) 268–278.
[164] S. Heinbuch, F. Dong, J.J. Rocca, E.R. Bernstein, Journal of Chemical Physics 133 (2010) 174314/1–174314/11.
[165] X.F. Duan, M. Page, Theochem: Journal of Molecular Structure 333 (1995) 233–242.
[166] S.P. Walch, Journal of Chemical Physics 99 (1993) 5295–5300.
[167] W.T. Wallace, R.L. Whetten, Journal of Physical Chemistry B 104 (2000) 10964–10968.
[168] X. Wu, L. Senapati, S.K. Nayak, A. Selloni, M. Hajaligol, Journal of Chemical Physics 117 (2002) 4010–4015.
[169] D. Stolcic, M. Fischer, G. Gantefor, Y.D. Kim, Q. Sun, P. Jena, Journal of the American Chemical Society 125 (2003) 2848–2849.
[170] B. Yoon, H. Hakkinen, U. Landman, A.S. Worz, J.M. Antonietti, S. Abbet, K. Judai, U. Heiz, Science 307 (2005) 403–407.
[171] Y.D. Kim, M. Fischer, G. Gantefor, Chemical Physics Letters 377 (2003) 170–176.
[172] J. Jansson, A.E.C. Palmqvist, E. Fridell, M. Skoglundh, L. Osterlund, P. Thormahlen, V. Langer, Journal of Catalysis 211 (2002) 387–397.
[173] J.-Y. Luo, M. Meng, Y.-Q. Zha, L.-H. Guo, Journal of Physical Chemistry C 112 (2008) 8694–8701.
[174] J.-Y. Luo, M. Meng, X. Li, X.-G. Li, Y.-Q. Zha, T.-D. Hu, Y.-N. Xie, J. Zhang, Journal of Catalysis 254 (2008) 310–324.
[175] C. Doornkamp, V. Ponec, Journal of Molecular Catalysis A 162 (2000) 19–32.
[176] P. Thormahlen, M. Skoglundh, E. Fridell, B. Andersson, Journal of Catalysis 188 (1999) 300–310.
[177] J. Jansson, Journal of Catalysis 194 (2000) 55–60.
[178] J. Jansson, M. Skoglundh, E. Fridell, P. Thormahlen, Topics in Catalysis 16 (2001) 385–389.
[179] E.-Y. Ko, E.D. Park, H.C. Lee, D. Lee, S. Kim, Angewandte Chemie International Edition 46 (2007) 734–737.
[180] F. Grillo, M.M. Natile, A. Glisenti, Applied Catalysis B: Environmental 48 (2004) 267–274.
[181] P. Li, D.E. Miser, S. Rabiei, R.T. Yadav, M.R. Hajaligol, Applied Catalysis B: Environmental 43 (2003) 151–162.
[182] A. Szegedi, M. Hegedus, J.L. Margitfalvi, I. Kiricsi, Chemical Communications (2005) 1441–1443.
[183] Y.H. Zheng, Y. Cheng, Y.S. Wang, F. Bao, L.H. Zhou, X.F. Wei, Y.Y. Zhang, Q. Zheng, Journal of Physical Chemistry B 110 (2006) 3093–3097.